3

Dynamics of radiative transport

Mário N. Berberan-Santos, Eduardo J. Nunes Pereira, and José M. G. Martinho
Instituto Superior Técnico, Portugal

3.1 INTRODUCTION

Radiative transfer, i.e. the transfer of energy mediated by real (as opposed to virtual) photons, is ubiquitous in Nature. For instance, the first step of photosynthesis consists of radiative transfer from the Sun's photosphere to the chlorophyll molecules of green plant leaves. The donor and acceptor are in this case 150 million kilometers apart, and the process takes eight minutes to be completed. Radiative transfer is also of importance in astrophysics, plasmas and in atomic and molecular luminescence, and it plays an important role in solar concentrators, discharge and fluorescent lamps, scintillation counters, and lasers.

The type of radiative transfer to be discussed in this chapter consists of the emission of a photon by an electronically excited molecule, with subsequent absorption by an identical ground-state molecule. It involves distances much smaller than those of the above example, and consequently occurs on much shorter timescales, usually determined by molecular excited-state lifetimes and not by photon propagation times.

In assemblies of like atoms or molecules, one elementary process of radiative transfer leads to another, until one of two things happens: (a) the excitation energy is irreversibly lost through a nonradiative path (internal conversion, intersystem crossing, quenching, etc.), or (b) the photon escapes from the sample (Fig. 3.1). This repeated radiative transfer is known by a number of names: radiative transport, radiative migration, self-absorption, reabsorption,

Resonance Energy Transfer. Edited by David L. Andrews and Andrey A. Demidov.

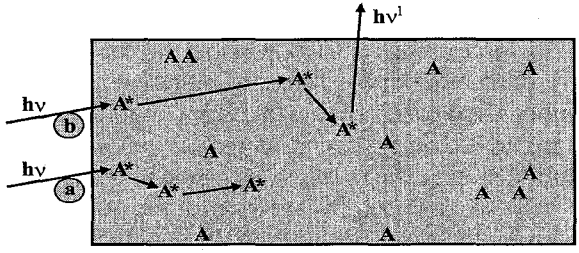

Figure 3.1 A schematic representation of the two kinds of photon trajectory. In case (a), the absorbed photon, of energy $h\nu$, never exits the sample, because the trajectory ends in a nonradiative decay process. In case (*b*), and after several reabsorptions, a photon of energy $h\nu'$ escapes from the enclosure.

radiation imprisonment, and radiation trapping. Its importance depends on many factors: the extent of spectral overlap between absorption and emission, absorption strength, fluorescence quantum yield, concentration, cell size and shape, excitation and detection geometries, etc. In the molecular case, it plays a particularly important role in solutions of highly fluorescent compounds with a good absorption–emission spectral overlap, whether concentrated or in large volumes. When present, radiative transport affects the measured fluorescence decays and spectra, as well as the fluorescence polarization. These observables are then functions of the excitation and emission wavelengths, concentration, and excitation and detection geometries.

When preparing this review, it was realized that the theoretical and experimental studies of radiative transport at a microscopic level have been conducted thus far in two almost noncommunicating areas, one concerned with atomic resonance radiation, mainly in the gas phase, and the other concerned with molecular fluorescence, mainly in the condensed phases. While there are aspects that are specific to each field, many concepts are common. Indeed, some remarkably similar results have been independently obtained in the two fields. In discussing molecular processes, mention of the relevant results obtained in the atomic field is therefore appropriate.

3.2 OVERVIEW OF ATOMIC AND MOLECULAR RADIATIVE TRANSPORT

3.2.1 Atomic resonance radiation

The first experimental study of radiative transport was made in 1912 by R. W. Wood [67], the discoverer of resonance radiation, with mercury vapor. He

observed that, upon continuous excitation of a given part of the vapor, 253.7 nm atomic mercury resonance radiation was emitted from a volume larger than that irradiated. By interposing a quartz window, he confirmed that the spread was due not to atomic motion, but rather to radiation scattering, by means of repeated absorptions and re-emissions. In 1923, Compton [23] put forward the first theory of radiative transport, considered by him as formally identical to gaseous diffusion: denoting the (base e) absorption coefficient of the medium by α, and by τ the average interval between absorption and emission of a quantum by an atom, the mean free path of the quanta is $1/\alpha$ and the effective average speed of the diffusing photons would be $1/(\alpha\tau)$. From these results, it followed that there was a "tendency of resonance radiation to remain imprisoned within a gas for a time which may be enormous in comparison with the time τ of imprisonment within individual atoms," in qualitative agreement with previous experimental observations. It was concluded that this effect should be important whenever the mean free path of the radiation was smaller than the dimensions of the apparatus (discharge tube). Compton's diffusion theory was later refined by Milne [43].

In 1927, Zemansky [68] carried out the first quantitative study of the phenomenon, again on the mercury 253.7 nm resonance line. He was able to show that the effective decay time of the radiation emitted in the central part of a discharge tube could be a thousand times greater than the intrinsic atomic state lifetime. An essential discrepancy between the experimental results and the Compton–Milne theory predictions was nevertheless found. Zemansky drew attention to several possible causes, including the effect of the line shape. However, he incorrectly assumed that "the radiation composing the whole absorption line diffused as a whole through the vapour," a mean absorption coefficient being thus applicable.

In 1932, Kenty [34] attempted to take into account the variation of the absorption over the frequency spectrum of the emission, by considering a Doppler line profile. He arrived at the surprising conclusion that, for an infinite medium, the average diffusion coefficient was infinite. This is indeed so, on account of the overwhelming contribution of the few photons originating at the band wings (that supposedly extend to infinite frequencies). This showed the general inapplicability of the diffusion equation to the radiative transport problem, an aspect that was, however, only clearly recognized in 1947, by Holstein [30, 31] and, independently, by Biberman [12]. Both derived a Boltzmann-type integro-differential equation for radiative transport, whose solution for a cutoff experiment was obtained by Holstein as a sum of time exponentials. An approximate solution, valid for sufficiently long times, was then given in terms of the slowest decaying exponential, whose argument was numerically obtained for two idealized enclosure geometries (infinite slab and infinite cylinder) and various spectral line shapes [30, 31]. Reasonable agreement with part of Zemansky's results was obtained. A refined experimental study of the mercury

253.7 nm line by Alpert, McCoubrey, and Holstein [2] yielded still better agreement, but also disclosed several complications not accounted for by the theory, namely the increasing contribution of collisional broadening with density.

Later studies of radiative transport in atomic gases have mainly dealt with refinements and experimental tests of approximate solutions to the Holstein–Biberman equation, taking into account aspects such as hyperfine structure [2, 62], simultaneous Doppler and Lorentz (collisional) broadening [62], Heisenberg (natural) broadening [32], incomplete frequency redistribution [50, 52, 54, 55], and inhomogeneous broadening [39]. Other works include approximate calculation of the full solution to the Holstein–Biberman equation, i.e. of the parameters in the sum of time exponentials (up to 20 terms), for the infinite slab [44, 60], for the infinite cylinder [45, 51, 61] and for the sphere [45], and the calculation of approximate solutions in the low-opacity region [20, 44], for which Holstein's long-time limit is of little use.

More recently, Wiorkowski and Hartmann developed and applied to experimental results [21, 64–66] a multiple scattering approach that allows calculation of the time dependence of the fluorescence, in response to an excitation pulse, in terms of an infinite series of unknown coefficients. The equivalence between this treatment and that based on the Holstein–Biberman equation has been shown [25, 36]. The multiple scattering approach is physically appealing, mathematically simpler and more flexible with respect to refinements. The unknown parameters of the theoretical decay law can be evaluated by Monte Carlo simulation [21, 64–66]. Lai, Liu, and Ma [36] have recently pointed out that, given the equivalence of the Holstein–Biberman equation and the multiple scattering method, the solution of this last treatment should asymptotically converge to the long-time exponential decay of the Holstein–Biberman equation. They then obtained formulas similar to those of the multiple scattering method directly from the Holstein–Biberman equation. Combining both types of solutions, it was shown that a single formula, with a finite number of terms, was able to reproduce both the short- and long-time behavior. The same result can also be used to obtain the steady state response of the system in terms of a finite sum [38].

3.2.2 Molecular fluorescence

Molecular radiative transport studies, theoretical or experimental, have not relied explicitly on the Holstein–Biberman equation. In fact, the only approximate solution of this equation known for many years, based on the fundamental mode, is often not appropriate to the molecular case. The typical molecular absorption coefficients and molecular absorption–emission overlaps are much smaller than those of atoms. Also, the fluorescence quantum yield is always smaller than unity. These three unfavorable factors render radiative

transport much less efficient in molecular ensembles than in atomic ensembles. As a consequence, the average macroscopic decay times of molecular ensembles seldom attain values more than three or four times the intrinsic lifetime – while for atoms, values one to three orders of magnitude higher than the intrinsic lifetime are common. In this way, molecular fluorescence decays under the influence of radiative transport are usually nonexponential, and show no signs of the fundamental mode – which manifests itself only at very late times, when the intensity is negligible.

In the molecular field, motivation for the study of radiative transport *per se* came from two applied subjects: scintillation counting [13, 15, 35] and analytic fluorescence spectrometry [37, 42, 49]. Particularly in the last case, reabsorption was, and still is, an unwanted complication in determination of the true fluorescence spectrum, quantum yield and lifetime. The first attempt to seriously model self-absorption was that of Birks [14]. He proposed an admittedly simple kinetic model to account for the increase of the macroscopic decay time. In this model, excited molecules were classified according to generation, and a common self-absorption probability was used for all photons. This implied an exponential decay. Later, Birks [17] recognized that the self-absorption probabilities of the successive generations were in general different, but failed to notice that the theoretical decay would no longer be exponential. Birks's approximate treatment was also presented in his influential reviews of molecular luminescence [16, 18, 19]. For this reason, and also because of the inherent simplicity, it became widely used; see, e.g., [5, 7, 24, 28, 53, 58].

Notwithstanding this, Kilin and Rozman [35], following a kinetic approach similar to that used later by Birks [16, 17, 19], had in 1959 obtained not only the correct (nonexponential) time dependence, rediscovered in 1985 by Wiorkowski and Hartmann [65] for the atomic case, but also the influence of self-absorption on the emission spectrum. However, their work remained little known until it was revived and extended [40, 41, 46]. Almost simultaneously, a similar approach, although lacking the emission wavelength dependence, was presented and applied to experimental results [33, 56, 57]. A stochastic theory of radiative transport was afterwards presented [10], allowing the calculation of all observables (including the time dependence of the polarization) from known parameters [10, 47]. This approach was recently refined and extended to include the contribution of nonradiative transport [11].

3.3 THE HOLSTEIN–BIBERMAN EQUATION

3.3.1 Delta-pulse excitation

Although derived with regard to the resonance radiation transport problem, this equation – slightly generalized – is equally appropriate for the molecular

case. Consider a given atomic or molecular ensemble, in a convex enclosure of otherwise arbitrary shape. Suppose that a small fraction of the ensemble is excited at time zero by a delta pulse, generating N_0 excited atoms or molecules, with a spatial distribution characterized by the number density $n(\vec{r}, t)$. Then, the time evolution of the number density of excited species $n(\vec{r}, t)$ will be given by

$$\frac{\partial n(\vec{r}, t)}{\partial t} = -\Gamma n(\vec{r}, t) + k_r \int_V f(\vec{r}, \vec{r}') n(\vec{r}', t) \mathrm{d}\vec{r}', \tag{3.1}$$

which is the Holstein–Biberman equation [12, 30]. In Eqn 3.1, the integration goes over the whole volume of the enclosure; Γ is the reciprocal atomic or molecular lifetime,

$$\Gamma = k_r + k_{nr} = \frac{1}{\tau_0}, \tag{3.2}$$

and k_r and k_{nr} are the radiative and nonradiative decay constants, respectively. In the atomic case, k_{nr} is due to quenching and is usually negligible. The function $f(\vec{r}, \vec{r}')$ is the average probability that a photon emitted by an excited atom or molecule at point $\vec{r}'$ will be absorbed by a ground-state atom or molecule in a unit volume element around point $\vec{r}$,

$$f(\vec{r}, \vec{r}') = \int_0^\infty F(\nu) k(\nu) \frac{1}{4\pi |\vec{r} - \vec{r}'|^2} \exp[-k(\nu) |\vec{r} - \vec{r}'|] \mathrm{d}\nu, \tag{3.3}$$

where $F(\nu)$ is the normalized emission spectrum, in the atomic case usually proportional to $k(\nu)$, the latter being the (base e) absorption coefficient of the medium.

Implicit in this derivation is: (i) neglect of the time of flight of the photons in comparison with the intrinsic lifetime τ_0. This is usually a very good approximation, breaking down only for very extended media of low opacity, where retardation effects are significant. Other usually valid approximations contained in Eqn 3.1 are (ii) neglect of boundary effects such as reflection or wall quenching, (iii) supposition of isotropic emission, (iv) assumption of spatial homogeneity of ground state species, and (v) neglect of material transport of excitation (diffusion, convection). Finally, (vi) complete frequency redistribution is assumed, i.e. a single emission frequency distribution $F(\nu)$ is valid for all atoms or molecules. This last approximation is not always valid, especially for atoms, and suitable extensions of Eqn 3.1 have been carried out [50, 52, 54, 55].

It is useful to define the spatial distribution function of excited species, $p(\vec{r}, t)$,

$$p(\vec{r},t)=\frac{n(\vec{r},t)}{\int_V n(\vec{r},t)\mathrm{d}\vec{r}}=\frac{n(\vec{r},t)}{N(t)}, \tag{3.4}$$

where $N(t)$ is the total number of excited atoms or molecules in the enclosure at time t. Using Eqn 3.4, Eqn 3.1 can be rewritten as

$$\frac{\partial p(\vec{r},t)}{\partial t}=k_r\left[\int_V f(\vec{r},\vec{r}')p(\vec{r}',t)\mathrm{d}\vec{r}'-p(\vec{r},t)\int_V\int_V f(\vec{r},\vec{r}')p(\vec{r},t)\mathrm{d}\vec{r}\,\mathrm{d}\vec{r}'\right]. \tag{3.5}$$

From Eqn 3.5 and, on physical grounds, one sees that a stationary spatial distribution is attained for long times, obeying, irrespective of the initial distribution,

$$p_s(\vec{r})=\frac{\int_V f(\vec{r},\vec{r}')p_s(\vec{r}')\mathrm{d}\vec{r}'}{\int_V\int_V f(\vec{r},\vec{r}')p_s(\vec{r}')\mathrm{d}\vec{r}\,\mathrm{d}\vec{r}'}. \tag{3.6}$$

Equation 3.6 can be rewritten as

$$p_s(\vec{r})=\frac{\alpha_s(\vec{r})}{\bar{\alpha}_s}, \tag{3.7}$$

where the numerator is the average probability that a photon, originating from an excited-state population distributed according to the stationary spatial distribution, will be absorbed in a unit volume element around point $\vec{r}$; the denominator is the average probability that a photon originating from an excited-state population distributed according to the same distribution will be absorbed.

From Eqns 3.1 and 3.4, and using the definition of $N(t)$, one obtains

$$-\frac{\mathrm{d}N}{\mathrm{d}t}=\left[\Gamma-k_r\int_V\int_V f(\vec{r},\vec{r}')p(\vec{r},t)\mathrm{d}\vec{r}\,\mathrm{d}\vec{r}'\right]N=[\Gamma-k_r\bar{\alpha}(t)]N, \tag{3.8}$$

where $\bar{\alpha}(t)$ is the probability that a photon originating from an excited-state population distributed according to the spatial distribution $p(\vec{r},t)$ will be absorbed. Integration of Eqn 3.8 gives

$$N(t)=N_0\exp(-\Gamma t)\exp\left[k_r\int_0^t\bar{\alpha}(u)\mathrm{d}u\right], \tag{3.9}$$

and hence the normalized (i.e. scaled to one at $t = 0$) decay of intensity of the radiation emitted by the enclosed ensemble, integrated over all directions, $\rho(t)$, is given by

$$\rho(t) = \frac{1 - \bar{\alpha}(t)}{1 - \bar{\alpha}_s(0)} \exp(-\Gamma t) \exp\left[k_r \int_0^t \bar{\alpha}(u) \mathrm{d}u\right]. \tag{3.10}$$

It follows, both from Eqn 3.10 and from the stabilization of the average absorption probability with time, that a single exponential decay will result for sufficiently long times, with a lifetime given by

$$\tau_s = \frac{\tau_0}{1 - \bar{\alpha}_s \Phi_0}, \tag{3.11}$$

where Φ_0 is the intrinsic emission quantum yield, $\Phi_0 = k_r/\Gamma = k_r \tau_0$.

In this way, to obtain the long-time limit solution of the radiative problem, one needs only to compute the average absorption probability corresponding to the long-time stationary distribution. This distribution can in turn be numerically obtained from Eqn 3.6, for each particular geometry, ground state density and line shape.

It may be noted that the maximum possible value for τ_s is attained for unit absorption probability in Eqn 3.11,

$$\tau_{s,max} = \frac{1}{k_{nr}}. \tag{3.12}$$

The general solution of Eqn 3.1 can be written as [30]

$$n(\vec{r}, t) = \sum_i n_i(\vec{r}) \mathrm{e}^{-\beta_i t}, \tag{3.13}$$

where the $n_i(\vec{r})$ are the stationary (but not necessarily positive for all values of $\vec{r}$) solutions of Eqn 3.1, and the β_i are the corresponding eigenvalues. The eigenvalue equation is obtained by insertion of Eqn 3.13 into Eqn 3.1, and takes the form

$$\Gamma n_i(\vec{r}) - k_r \int_V f(\vec{r}, \vec{r}') n_i(\vec{r}') \mathrm{d}\vec{r}' = \beta_i n_i(\vec{r}). \tag{3.14}$$

Integrating both sides of Eqn. 3.14 over space, one obtains, for the eigenvalues,

$$\beta_i = \Gamma - k_r \bar{\alpha}_i, \tag{3.15}$$

where the generalized absorption probability $\bar{\alpha}_i$ is

$$\bar{\alpha}_i = \int_V \int_V f(\vec{r}, \vec{r}') p_i(\vec{r}') \mathrm{d}\vec{r}\, \mathrm{d}\vec{r}', \tag{3.16}$$

and the generalized distribution function $p_i(\vec{r})$ is

$$p_i(\vec{r}) = \frac{n_i(\vec{r})}{\int_V n_i(\vec{r}) \mathrm{d}\vec{r}} = \frac{n_i(\vec{r})}{N_i}. \tag{3.17}$$

Insertion of Eqn 3.15 into the eigenvalue equation 3.14, rewritten in terms of the generalized distribution functions $p_i(\vec{r})$, shows that these functions are solutions of Eqn 3.6, i.e. they are indeed stationary distributions. Like the stationary solutions $n_i(\vec{r})$, these generalized distributions may take negative values, which are again devoid of direct physical meaning, except for the long-time solution, $p_s(\vec{r})$, that belongs to the smallest eigenvalue, $\beta_s = 1/\tau_s$, which is always positive.

From Eqns 3.13–3.17, the time-dependent distribution function can be written as

$$p(\vec{r}, t) = \frac{\sum_i \left(\int_V n_i(\vec{r}) \mathrm{d}\vec{r} \right) p_i(\vec{r}) \mathrm{e}^{k_r \bar{\alpha}_i t}}{\sum_i \left(\int_V n_i(\vec{r}) \mathrm{d}\vec{r} \right) \mathrm{e}^{k_r \bar{\alpha}_i t}} = \frac{\sum_i N_i p_i(\vec{r}) \mathrm{e}^{k_r \bar{\alpha}_i t}}{\sum_i N_i \mathrm{e}^{k_r \bar{\alpha}_i t}} = \frac{\sum_i c_i p_i(\vec{r}) \mathrm{e}^{k_r \bar{\alpha}_i t}}{\sum_i c_i \mathrm{e}^{k_r \bar{\alpha}_i t}}, \tag{3.18}$$

the coefficients c_i being the fraction of the excited population associated with the ith eigenvalue,

$$c_i = \frac{N_i}{N_0} \quad (i = 1, 2, \ldots). \tag{3.19}$$

Using $\bar{\alpha}(t)$ as defined for Eqn 3.8, one obtains, from Eqn 3.18,

$$\bar{\alpha}(t) = \frac{\sum_i c_i \bar{\alpha}_i \mathrm{e}^{k_r \bar{\alpha}_i t}}{\sum_i c_i \mathrm{e}^{k_r \bar{\alpha}_i t}}, \tag{3.20}$$

and inserting it in Eqn 3.10, this yields the sought-for solution:

$$\rho(t) = \exp(-\Gamma t) \sum_i a_i \exp(k_r \bar{\alpha}_i t) = \sum_i a_i \exp(-\beta_i t) = \sum_i a_i \exp(-t/\tau_i), \tag{3.21}$$

Equation 3.26 becomes, after normalization,

$$\rho(t, \vec{r}_b) = \sum_i \alpha_{bi} e^{-\beta_i t}, \tag{3.28}$$

where

$$a_{bi} = \frac{(1 - \bar{\alpha}_{bi})c_i}{\sum_i (1 - \bar{\alpha}_{bi})c_i}, \tag{3.29}$$

and is similar in form to the overall decay, Eqn. 3.21.

A further case of interest is the direction- and frequency-resolved decay. This experimental situation is much less common in atomic than in molecular spectroscopy, probably on account of the much smaller emission spectral width. Such a decay is obtained from Eqn 3.26 by just removing the integration over frequencies carried out in Eqn 3.27:

$$\rho(t, \nu, \vec{r}_b) = \sum_i a_{bi}(\nu) e^{-\beta_i t}, \tag{3.30}$$

where

$$a_{bi}(\nu) = \frac{[1 - \bar{\alpha}_{bi}(\nu)]c_i}{\sum_i [1 - \bar{\alpha}_{bi}(\nu)]c_i}, \tag{3.31}$$

and where

$$\bar{\alpha}_{bi}(\nu) = \int_V \alpha_b(\vec{r}, \nu) n_i(\vec{r}) d\vec{r}, \tag{3.32}$$

with

$$\alpha_b(\vec{r}, \nu) = \int_0^{|\vec{r}_b - \vec{r}|} k(\nu) \exp[-k(\nu)x] dx. \tag{3.33}$$

3.3.2 Continuous excitation (photostationary state)

For decays in response to temporal profiles other than delta excitation, and still under the assumption of nonsaturating conditions, the decay is obtained from linear response theory as the convolution of the excitation profile with the delta

where

$$a_i = \frac{(1-\bar{\alpha}_i)c_i}{\sum_i (1-\bar{\alpha}_i)c_i} \tag{3.22}$$

and

$$\tau_i = \frac{\tau_0}{1-\bar{\alpha}_i \Phi_0}. \tag{3.23}$$

The average decay time $\bar{\tau}$ is therefore

$$\bar{\tau} = \sum_i b_i \tau_i, \tag{3.24}$$

with

$$b_i = \left(\frac{1-\bar{\alpha}_i}{1-\bar{\alpha}_i \Phi_0} c_i\right) \Big/ \left(\sum_i \frac{1-\bar{\alpha}_i}{1-\bar{\alpha}_i \Phi_0} c_i\right). \tag{3.25}$$

In this way, $\bar{\tau}$ reduces to τ_s only when $b_s \simeq 1$.

In most experiments, the measured decay corresponds to a given direction or solid angle, and not to the integrated signal over the surface of the enclosure. In such a case, and unless the excitation process and the enclosure geometry are such as to preserve a high symmetry (e.g. excitation along the central axis of a long cylinder), the decay will be a function of the direction of observation. Considering, for instance, that the recorded signal corresponds to the photons reaching a given point $\vec{r}_b$ at the system's boundary, the decay will be

$$\rho(t, \vec{r}_b) \propto \int_V [1-\alpha_b(\vec{r})] n(\vec{r}, t) \mathrm{d}\vec{r} = \sum_i N_i (1-\bar{\alpha}_{bi}) \mathrm{e}^{-\beta_i t}, \tag{3.26}$$

where $\alpha_b(\vec{r})$ is the average probability that a photon emitted by an excited atom or molecule at point $\vec{r}$, and toward $\vec{r}_b$, will be absorbed by a ground-state atom or molecule before reaching the enclosure's surface at $\vec{r}_b$:

$$\alpha_b(\vec{r}) = \int_0^{|\vec{r}_b - \vec{r}|} \int_0^{\infty} F(\nu) k(\nu) \exp[-k(\nu)x] \mathrm{d}\nu \, \mathrm{d}x. \tag{3.27}$$

response function (e.g. [8] and references therein). For continuous excitation, the steady state intensity is in this way shown to be proportional to $\sum_i a_i/\beta_i$, and we obtain, for the overall intensity I,

$$\frac{I}{I_0} = \frac{\Phi}{\Phi_0} = \sum_i c_i \frac{1 - \bar{\alpha}_i}{1 - \bar{\alpha}_i \Phi_0}, \tag{3.34}$$

where I_0 is the intensity expected in the absence of radiative transport, and Φ is the macroscopic emission quantum yield.

As might be expected, radiative transport causes a decrease in the overall intensity only when the intrinsic emission quantum yield is smaller than one. In such a case, the decrease may be strong, even for moderate optical densities, owing to the nonlinear dependence on Φ_0. In this regard, Eqn 3.34 can be made clearer by rewriting it as

$$\frac{\Phi}{\Phi_0} = \sum_i c_i (1 - \bar{\alpha}_i) \left[1 + \bar{\alpha}_i \Phi_0 + (\bar{\alpha}_i \Phi_0)^2 + (\bar{\alpha}_i \Phi_0)^3 + \ldots\right], \tag{3.35}$$

where the first term in brackets corresponds to the escape probability for the ith eigenmode, whose photons may suffer zero, one, two, three, etc. reabsorptions before escape.

Similarly, for the direction-resolved case, the steady state intensity, obtained from Eqn 3.30, is given by

$$\frac{I_b}{I_{0b}} = \frac{\Phi_b}{\Phi_0} = \sum_i c_i \frac{1 - \bar{\alpha}_{bi}}{1 - \bar{\alpha}_i \Phi_0}. \tag{3.36}$$

Now, some $\bar{\alpha}_{bi}$ may be negative, in such a way that, for some directions, the apparent quantum yield of emission will be larger than the intrinsic one. Of course, a compensation will exist, so that the integrated yield over all directions will be according to Eqn 3.34, as follows from Eqn 3.36.

Finally, for the direction- and frequency-resolved cases, one obtains for the steady state

$$I_b(\nu) = I_{0b} F(\nu) \sum_i c_i \frac{1 - \alpha_{bi}(\nu)}{1 - \bar{\alpha}_i \Phi_0}. \tag{3.37}$$

This equation can be used to account for the deformation of spectral shape caused by radiative transport. In the atomic case, this effect is known as self-reversal [22, pp. 62–65] (Fig. 3.2). In the molecular case, there is a strong decrease in the blue side of the emission, the only side to significantly overlap absorption (Fig. 3.3).

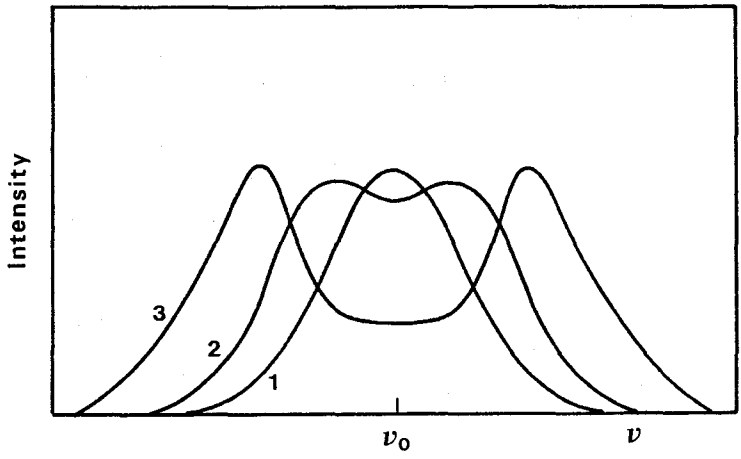

Figure 3.2 A schematic representation of atomic resonance line self-reversal. Curve 1 is the intrinsic absorption and emission spectrum. Increase of the atomic concentration leads to a progressive deformation of the emission spectrum (curves 2 and 3) to the point of yielding two apparently distinct lines.

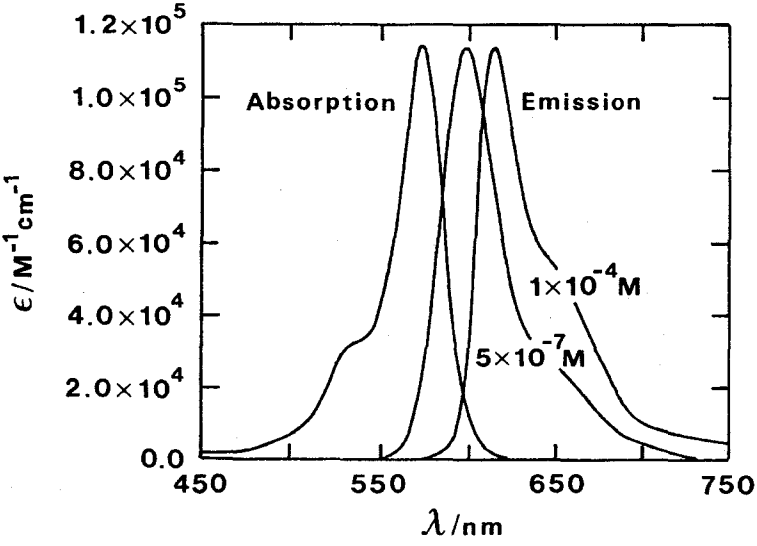

Figure 3.3 Absorption and fluorescence spectra (1 cm cell, right-angle geometry, excitation wavelength 530 nm) of the dye rhodamine 101 in acidified ethanol. Fluorescence spectra are normalized at the maximum. The emission spectrum of the concentrated solution shows a noticeable decrease of intensity on its blue side.

As mentioned above, with the exception of the long-time solution (corresponding to the eigenvalue β_s), all eigenfunctions take negative values at some points, and cannot thus be identified with physical distributions. This has been considered a drawback of the Holstein solution, being based on modes of difficult physical interpretation [21, 25, 36, 38, 64–66]. In fact, the negative values are essential to account for the possibility of rise times and increased apparent quantum yields of emission in some directions of space. These, in turn, have a clear meaning (see Section 3.5). Nevertheless, the original solution of the Holstein–Biberman equation, as given by Holstein, suffers from some real limitations: (i) the eigenvalues and eigenfunctions are not easily calculated; and (ii) it cannot be used to obtain the polarization of the emitted radiation. The approaches described in the next two sections overcome these difficulties.

3.4 MULTIPLE SCATTERING REPRESENTATION

3.4.1 Connection with the Holstein–Biberman equation

As mentioned in Section 3.2, Lai, Liu, and Ma [36] showed that the solution to the Holstein–Biberman equation could be given in a form alternative to that of Holstein's [30]. Rewriting Eqn 3.1 as

$$\frac{\partial n(\vec{r},t)}{\partial t} = (-\Gamma + k_r \mathbf{L}) n(\vec{r},t), \tag{3.38}$$

where the operator $\mathbf{L}$ is

$$\mathbf{L}[n(\vec{r},t)] = \int_V f(\vec{r},\vec{r}\,') n(\vec{r}\,',t) \mathrm{d}\vec{r}\,', \tag{3.39}$$

the symbolic solution of Eqn 3.38 is therefore

$$n(\vec{r},t) = \exp(-\Gamma t + k_r t\mathbf{L}) n(\vec{r},0) = \exp(-\Gamma t)\exp(k_r t\mathbf{L}) n(\vec{r},0), \tag{3.40}$$

where the exponential of an operator $\mathbf{A}$ is defined as

$$\exp(\mathbf{A}) = 1 + \mathbf{A} + \frac{\mathbf{AA}}{2} + \frac{\mathbf{AAA}}{3!} + \ldots. \tag{3.41}$$

Equation 3.40 thus becomes [36]

$$n(\vec{r},t) = \mathrm{e}^{-\Gamma t} \sum_{i=0}^{\infty} n_i(\vec{r}) \frac{(k_r t)^i}{i!}, \tag{3.42}$$

with

$$n_i(\vec{r}) = \mathbf{L}^i n(\vec{r}, 0). \tag{3.43}$$

It follows from Eqn 3.43 that

$$n_{i+1}(\vec{r}) = \mathbf{L} n_i(\vec{r}). \tag{3.44}$$

From Eqn 3.42, the spatial distribution function $p(\vec{r}, t)$ can be computed as

$$p(r, t) = \left[\sum_i n_i(\vec{r}) \frac{(k_r t)^i}{i!}\right] \Bigg/ \left[\sum_i N_i \frac{(k_r t)^i}{i!}\right], \tag{3.45}$$

and the time-dependent absorption probability as

$$\bar{\alpha}(t) = \left[\sum_i N_{i+1} \frac{(k_r t)^i}{i!}\right] \Bigg/ \left[\sum_i N_i \frac{(k_r t)^i}{i!}\right], \tag{3.46}$$

hence, from Eqn 3.10, and in agreement with [25],

$$\rho(t) = \mathrm{e}^{-\Gamma t} \sum_{i=0}^{\infty} \frac{N_i - N_{i+1}}{N_0 - N_1} \frac{(k_r t)^i}{i!}. \tag{3.47}$$

It is seen that numerical values for this solution to the Holstein–Biberman equation can be obtained more easily than for that based on the eigenvalues. However, the asymptotic behavior toward a single exponential is not apparent from Eqn 3.47, and so computation of the solution for long times may demand a prohibitive number of terms. A remedy for this situation was proposed in [36] (see Eqn 3.66 below).

3.4.2 Kinetic model

The terms of the expansion given in Eqn 3.47 admit a simple physical interpretation: each corresponds to a given generation of excited atoms or molecules. More specifically, the ith term corresponds to the ith generation. It is in fact possible to directly obtain an equation with the same time- dependence as Eqn 3.47 from a kinetic model that considers the various generations, without invoking the Holstein–Biberman equation [35, 41, 65]. To do so, it is convenient to consider the following kinetic scheme:

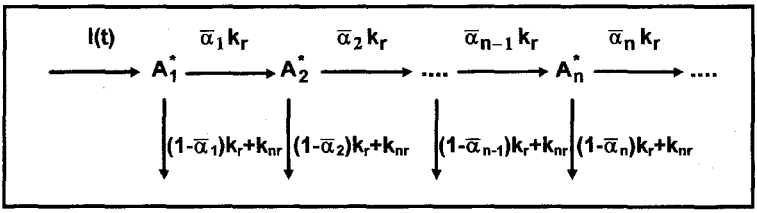

where $N_1(t)$ is the number of first-generation molecules, directly excited by the pulse $I(t)$, $N_2(t)$ is the number of second-generation molecules, excited by absorption of the photons emitted by the first-generation molecules, etc., and $\bar{\alpha}_i$ is the average absorption probability of photons emitted by ith generation molecules. For delta-pulse excitation, one obtains [35, 41, 65]:

$$N_i(t) = N_0 a_i \frac{(k_r t)^{i-1}}{(i-1)!} \exp(-\Gamma t), \tag{3.48}$$

with

$$a_i = \prod_{j=1}^{i-1} \bar{\alpha}_j \qquad (a_1 = 0). \tag{3.49}$$

The intensity due to N_i that will reach the boundary, at a given point $\vec{r}_b$, and for a given emission wavelength λ, will be

$$I_{bi}(\lambda, t) = k_r[1 - \alpha_{bi}(\lambda)] N_i(t). \tag{3.50}$$

Hence the total emission intensity is

$$I_b(\lambda, t) = \sum_{i=1}^{\infty} I_{bi}(\lambda, t) = k_r N_0 \sum_{i=1}^{\infty} [1 - \alpha_{bi}(\lambda)] \left(\prod_{j=1}^{i-1} \bar{\alpha}_j \right) \frac{(k_r t)^{i-1}}{(i-1)!} \exp(-\Gamma t), \tag{3.51}$$

and the decay will be

$$\rho_b(\lambda, t) = \mathrm{e}^{-\Gamma t} \sum_{i=1}^{\infty} \frac{1 - \alpha_{bi}(\lambda)}{1 - \alpha_{b0}(\lambda)} a_i \frac{(k_r t)^{i-1}}{(i-1)!}, \tag{3.52}$$

while for the emission integrated over wavelengths and directions the decay is

$$\rho(t) = \mathrm{e}^{-\Gamma t} \sum_{i=1}^{\infty} \frac{1 - \bar{\alpha}_i}{1 - \bar{\alpha}_1} a_i \frac{(k_r t)^{i-1}}{(i-1)!}. \tag{3.53}$$

This equation is identical to Eqn 3.47, as will be shown in Section 3.5. However, a physically clearer approach, without the involvement of unknown parameters, is desirable. We describe this in the next section.

3.5 STOCHASTIC APPROACH

3.5.1 Formulation and delta-pulse response

Consider the absorption of a photon at $t = 0$, according to a given spatial distribution $P_1(\vec{r})$. The excited molecule generated at time $t = 0$ will relax to the ground state, yielding a probability $p_n(\lambda, t)$ that, between t and $t + \mathrm{d}t$, a photon with wavelength λ will hit the boundary at point $\vec{r}_b$ and thus leave the sample (neglecting reflection). This probability can be written as

$$p_b(\lambda, t) = \sum_{n=1}^{\infty} p_{bn}(\lambda, t), \tag{3.54}$$

where $p_{bn}(\lambda, t)$ is the probability that a photon with wavelength λ will cross the boundary at a point $\vec{r}_b$, between t and $t + \mathrm{d}t$, after exactly n absorption–emission events. This probability can in turn be written as

$$p_{bn}(\lambda, t) = f_{bn}(\lambda) g_n(t), \tag{3.55}$$

where $f_{bn}(\lambda)$ is the probability that a photon with wavelength λ will hit the boundary at point $\vec{r}_b$ (thus leaving the sample), after exactly n absorption–emission events, and $g_n(t)$ is the probability that an nth-generation molecule will emit a photon between t and $t + \mathrm{d}t$, given that it will emit one. Assuming that the photon propagation time is negligible, this probability (the normalized density function) is given by (see Appendix A)

$$g_n(t) = \Gamma \frac{(\Gamma t)^{n-1}}{(n-1)!} \mathrm{e}^{-\Gamma t}. \tag{3.56}$$

The probability $f_{bn}(\lambda)$ is

$$f_{bn}(\lambda) = \frac{1}{4\pi} \Phi_0 F(\lambda) \int_V [1 - \alpha_b(\vec{r}, \lambda)] P_n(\vec{r}) \mathrm{d}\vec{r}, \tag{3.57}$$

where $\alpha_b(\vec{r}, \lambda)$ is given by Eqn 3.33 and $P_n(\vec{r})$, the probability that an nth-generation photon will be emitted at $\vec{r}$, is

$$P_n(\vec{r}) = \int_V \int_V \cdots \int_V f(\vec{r}, \vec{r}_{n-1})\, \Phi_0 f(\vec{r}_{n-1}, \vec{r}_{n-2}) \cdots \Phi_0 f(\vec{r}_2, \vec{r}_1) P_1(\vec{r}_1) \mathrm{d}\vec{r}_{n-1}\, \mathrm{d}\vec{r}_{n-2} \cdots \mathrm{d}\vec{r}_1, \tag{3.58}$$

with $f(\vec{r}, \vec{r}')$ given by Eqn 3.3. Equation 3.58 can be written as a recurrence relation:

$$P_{n+1}(\vec{r}) = \Phi_0 \int_V f(\vec{r}, \vec{r}_n) P_n(\vec{r}_n) \mathrm{d}\vec{r}_n. \tag{3.59}$$

From it, one obtains the spatial distribution function $p_n(\vec{r})$ of the nth generation,

$$p_n(\vec{r}) = \frac{P_n(\vec{r})}{\int_V P_n(\vec{r}) \mathrm{d}\vec{r}} = \frac{\int_V f(\vec{r}, \vec{r}_{n-1}) p_{n-1}(\vec{r}_{n-1}) \mathrm{d}\vec{r}_{n-1}}{\int_V \int_V f(\vec{r}, \vec{r}_{n-1}) p_{n-1}(\vec{r}_{n-1}) \mathrm{d}\vec{r}_{n-1}\, \mathrm{d}\vec{r}}, \tag{3.60}$$

which shows the equivalence between this approach and that based on the Holstein–Biberman equation (compare with Eqns 3.6 and 3.44).

The normalized decay law will thus be

$$\rho_b(\lambda, t) = \frac{p_b(\lambda, t)}{p_b(\lambda, 0)} = \mathrm{e}^{-\Gamma t} \sum_{n=1}^{\infty} \frac{\int_V [1 - \alpha_b(\vec{r}, \lambda)] P_n^0(\vec{r}) \mathrm{d}\vec{r}}{\int_V [1 - \alpha_b(\vec{r}, \lambda)] P_1^0(\vec{r}) \mathrm{d}\vec{r}} \frac{(k_r t)^{n-1}}{(n-1)!}, \tag{3.61}$$

where $P_i^0(\vec{r})$ denotes $P_i(\vec{r})$ when $\Phi_0 = 1$. Using Eqn 3.60,

$$\rho_b(\lambda, t) = \mathrm{e}^{-\Gamma t} \sum_{n=1}^{\infty} \frac{1 - \alpha_{bn}(\lambda)}{1 - \alpha_{b1}(\lambda)} \frac{\int_V P_n^0(\vec{r}) \mathrm{d}\vec{r}}{\int_V P_1^0(\vec{r}) \mathrm{d}\vec{r}} \frac{(k_r t)^{n-1}}{(n-1)!}; \tag{3.62}$$

Taking into account Eqns 3.59 and 3.60 and the definition of $\bar{\alpha}_i$ (see Eqn 3.16) one has

$$\frac{\int_V P_n^0(\vec{r}) \mathrm{d}\vec{r}}{\int_V P_1^0(\vec{r}) \mathrm{d}\vec{r}} = \prod_{i=1}^{n-1} \bar{\alpha}_i \tag{3.63}$$

and Eqn 3.62 becomes identical to Eqn 3.52,

$$\rho_b(\lambda, t) = \mathrm{e}^{-\Gamma t} \sum_{n=1}^{\infty} \frac{1-\alpha_{bn}(\lambda)}{1-\alpha_{b1}(\lambda)} \prod_{i=1}^{n-1} \bar{\alpha}_i \frac{(k_r t)^{n-1}}{(n-1)!}. \tag{3.64}$$

The emission integrated over wavelengths and directions is

$$\begin{aligned}\rho(t) &= \mathrm{e}^{-\Gamma t} \sum_{n=1}^{\infty} \frac{\int_V P_n^0(\vec{r})\mathrm{d}\vec{r} - \int_V \int_V f(\vec{r},\vec{r}') P_n^0(\vec{r})\mathrm{d}\vec{r}\,\mathrm{d}\vec{r}'}{\int_V P_1^0(\vec{r})\mathrm{d}\vec{r} - \int_V \int_V f(\vec{r},\vec{r}') P_1^0(\vec{r})\mathrm{d}\vec{r}\,\mathrm{d}\vec{r}'} \frac{(k_r t)^{n-1}}{(n-1)!} \\ &= \mathrm{e}^{-\Gamma t} \sum_{n=1}^{\infty} \frac{1-\bar{\alpha}_n}{1-\bar{\alpha}_1} \frac{\int_V P_n^0(\vec{r})\mathrm{d}\vec{r}}{\int_V P_1^0(\vec{r})\mathrm{d}\vec{r}} \frac{(k_r t)^{n-1}}{(n-1)!}.\end{aligned} \tag{3.65}$$

Using Eqn 3.63 again, Eqn 3.65 becomes identical to Eqn 3.53.

Knowing that a stationary distribution is reached for the higher generations ($\bar{\alpha}_n \to \bar{\alpha}_s$), one obtains

$$\begin{aligned}\rho(t) &= \mathrm{e}^{-\Gamma t} \sum_{n=1}^{\infty} \frac{1-\bar{\alpha}_n}{1-\bar{\alpha}_1} \prod_{i=1}^{n-1} \bar{\alpha}_i \frac{(k_r t)^{n-1}}{(n-1)!} \\ &\simeq \mathrm{e}^{-\Gamma t} \sum_{n=1}^{m} \frac{1-\bar{\alpha}_n}{1-\bar{\alpha}_1} \prod_{i=1}^{n-1} \bar{\alpha}_i \frac{(k_r t)^{n-1}}{(n-1)!} + \mathrm{e}^{-\Gamma t} \sum_{n=m+1}^{\infty} \frac{1-\bar{\alpha}_S}{1-\bar{\alpha}_1} \left(\prod_{i=1}^{m} \bar{\alpha}_i\right) \bar{\alpha}_S^{n-m-1} \frac{(k_r t)^{n-1}}{(n-1)!} \\ &= \mathrm{e}^{-\Gamma t} \sum_{n=1}^{m} \frac{1-\bar{\alpha}_n}{1-\bar{\alpha}_1} \prod_{i=1}^{n-1} \bar{\alpha}_i \frac{(k_r t)^{n-1}}{(n-1)!} + \mathrm{e}^{-\Gamma t} \frac{1-\bar{\alpha}_S}{1-\bar{\alpha}_1} \left(\prod_{i=1}^{m} \frac{\bar{\alpha}_i}{\bar{\alpha}_S}\right) \sum_{n=m+1}^{\infty} \bar{\alpha}_S^{n-m-1} \frac{(k_r \bar{\alpha}_S t)^{n-1}}{(n-1)!} \\ &= \mathrm{e}^{-\Gamma t} \left[\sum_{n=1}^{m} \frac{1-\bar{\alpha}_n}{1-\bar{\alpha}_1} \left(\prod_{i=1}^{n-1} \bar{\alpha}_i\right) \frac{(k_r t)^{n-1}}{(n-1)!} - \frac{1-\bar{\alpha}_S}{1-\bar{\alpha}_1} \left(\prod_{i=1}^{m} \frac{\bar{\alpha}_i}{\bar{\alpha}_S}\right) \sum_{n=m+1}^{\infty} \frac{(k_r \bar{\alpha}_S t)^{n-1}}{(n-1)!} \right] \\ &\quad + \frac{1-\bar{\alpha}_S}{1-\bar{\alpha}_1} \left(\prod_{i=1}^{m} \frac{\bar{\alpha}_i}{\bar{\alpha}_S}\right) \mathrm{e}^{(k_r \bar{\alpha}_S - \Gamma)t},\end{aligned} \tag{3.66}$$

which shows that a long-time exponential is asymptotically attained. The approximation made in Eqn 3.66 is of course better the higher m is. A similar approximation holds for Eqn 3.64. The usefulness of this approach has been demonstrated [36].

Some experimental results [48] and their comparison with theoretic predictions are now presented. The systems to be discussed are solutions of the fluorescent dye rhodamine 101 in acidified ethanol or ethanol–methanol (9 : 1 v/v) ($\Phi_0 = 0.9$ and $\tau_0 = 4.3$ ns at room temperature), whose absorption and

emission spectra are depicted in Fig. 3.3. The enclosure under consideration is a typical 1 cm × 1 cm fluorescence cell. Two common detection geometries are considered: front-face (30°/60°) and right-angle (see Fig. 3.4).

The fluorescence decay of a 10^{-3} M solution of rhodamine 101, recorded with the front-face geometry, is shown in Fig. 3.5. The decay is nonexponential and the average lifetime is almost the double of the intrinsic lifetime. The fit to the theoretical decay, Eqn. 3.64, is quite good. In Fig. 3.6 a comparison is made between the experimental and calculated average lifetimes (from the equation, with the amplitudes evaluated by Monte Carlo simulation [47]). Again, there is a general agreement between experiment and theory [48]. The observed trend with emission wavelength deserves a comment: the average lifetime is lower in the overlap region than in the red side of the emission. This occurs because "blue" photons are either emitted close to the boundary, at early times, or are reabsorbed, later to appear as "red" photons.

The fluorescence decay of a 5×10^{-4} M solution of rhodamine 101 shown in Fig. 3.7, recorded with right-angle geometry, displays a significant rise time. The fit to the theoretical decay, Eqn. 3.64, is quite good. In Fig. 3.8 a comparison is made between the experimental and calculated average lifetimes (again with amplitudes evaluated by Monte Carlo simulation [47]). It is seen that the agreement between experiment and theory is good [48]. The observed trend

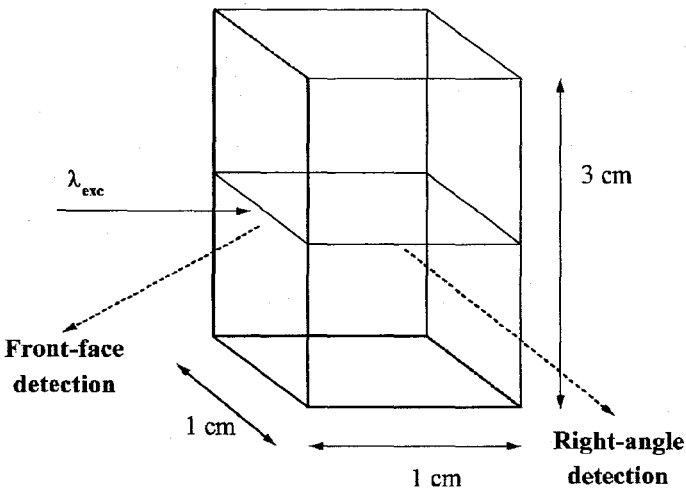

Figure 3.4 Experimental excitation and emission geometries, also reproduced in the Monte Carlo simulations. The enclosure size and shape correspond to a typical fluorescence cell. (Reprinted with permission from E. J. Nunes Pereira, M. N. Berberan-Santos, and J. M. G. Martinho, *J. Chem. Phys.* 104 (1996) 8950. Copyright 1996 American Institute of Physics.)

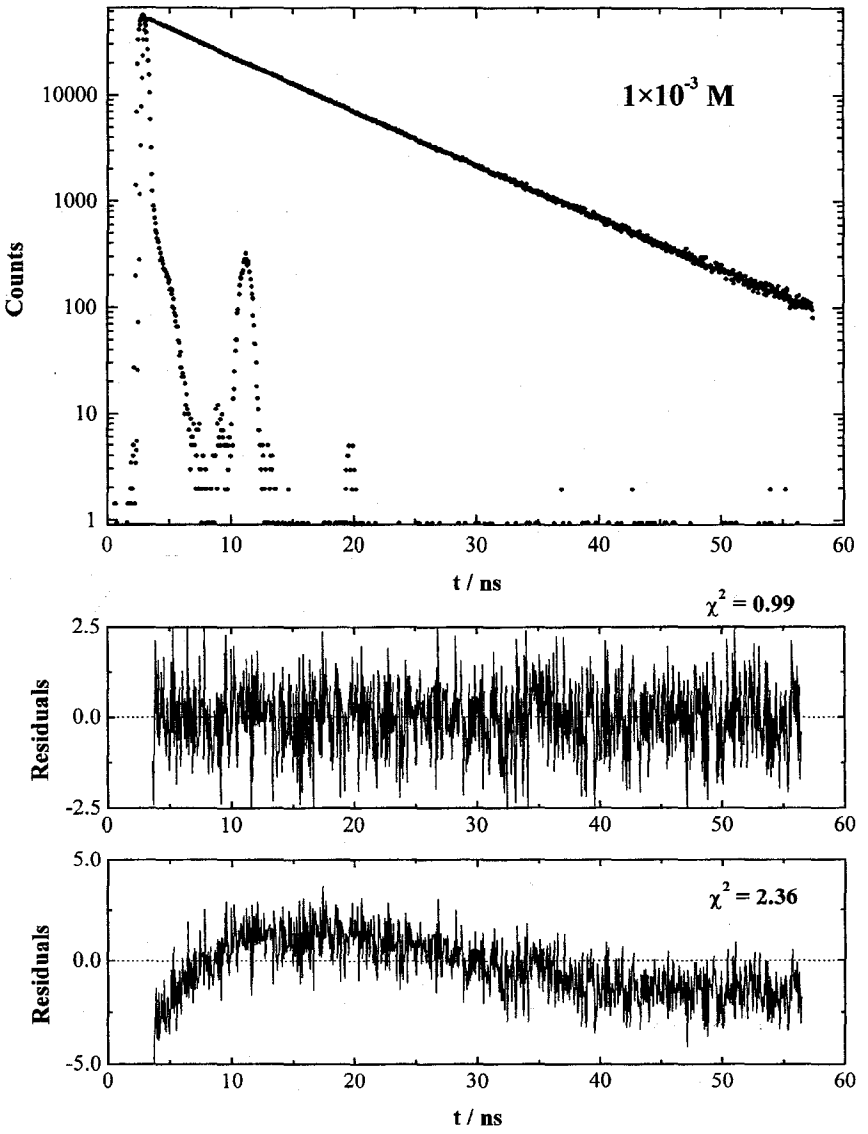

Figure 3.5 The fluorescence decay of a 10^{-3} M solution of rhodamine 101 in ethanol, at room temperature, front-face geometry. Excitation wavelength 294 nm; emission wavelength 620 nm. The average decay time is 8.4 ns. The fit to Eqn 3.64, with the intrinsic lifetime fixed at the dilute solution value of 4.34 ns, is quite good (upper residuals plot and reduced chi-squared value), while the fit to a single exponential is poor (lower residuals plot and reduced chi-squared value.)

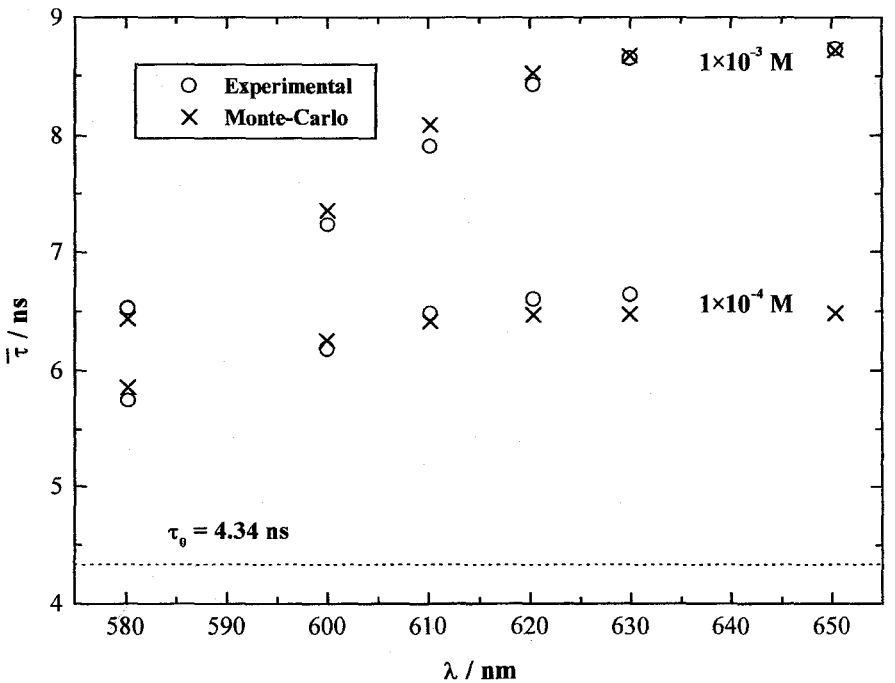

Figure 3.6 A comparison of experimental and predicted average lifetimes of rhodamine 101 for the front-face geometry, as a function of concentration and emission wavelength. Excitation wavelength 294 nm.

with emission wavelength is, however, opposite to that observed in front-face: the average lifetime is higher in the overlap region than in the red side of the emission. This occurs because "blue" photons, often absorbed, on average suffer more reabsorptions than "red" photons, on their way to the detector. The rise time, only observed in the blue [47], precisely reflects this waiting time for the arrival of "blue" photons. Holstein's solution of the Holstein–Biberman equation, in terms of eigenfunctions, provides for the rise times through negative amplitudes for some eigenmodes, at some points of space, as discussed in Section 3.3.2.

The physical picture can be made clearer by considering the spatial distribution of several generations of excited molecules, obtained by Monte Carlo simulation [47], as shown in Figs 3.9 and 3.10. As can be seen, the distribution of first-generation molecules is dictated by both the direction of the excitation beam and the opacity of the medium at the excitation wavelength, which controls its penetration. Excitation "diffusion" is more or less rapid according to the opacity in the spectral overlap region. For the front-face geometry

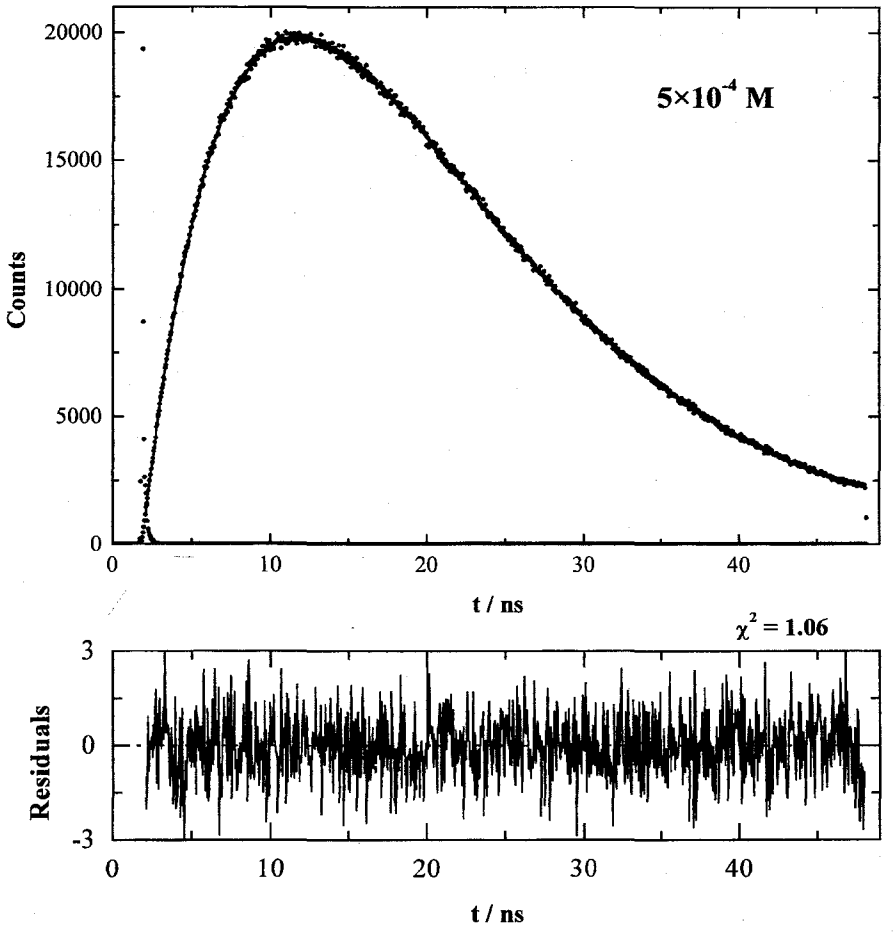

Figure 3.7 The fluorescence decay of a 5×10^{-4} M solution of rhodamine 101 in ethanol, at room temperature; right-angle geometry. Excitation wavelength 300 nm; emission wavelength 576 nm. There is a pronounced rise time. The fit to Eqn 3.64, with the intrinsic lifetime fixed at the dilute solution value of 4.34 ns, is quite good (residuals plot and reduced chi-squared value).

(Fig. 3.9), excited molecules are initially close to the boundary point for which emission is recorded, and then diffuse away from it. On the contrary, for the right-angle geometry (Fig. 3.10), excited molecules are initially far from the boundary point for which emission is recorded, but become closer over time. Only for very high generations (and whose contribution to the decay is very small), is the distribution close to the stationary distribution, corresponding to

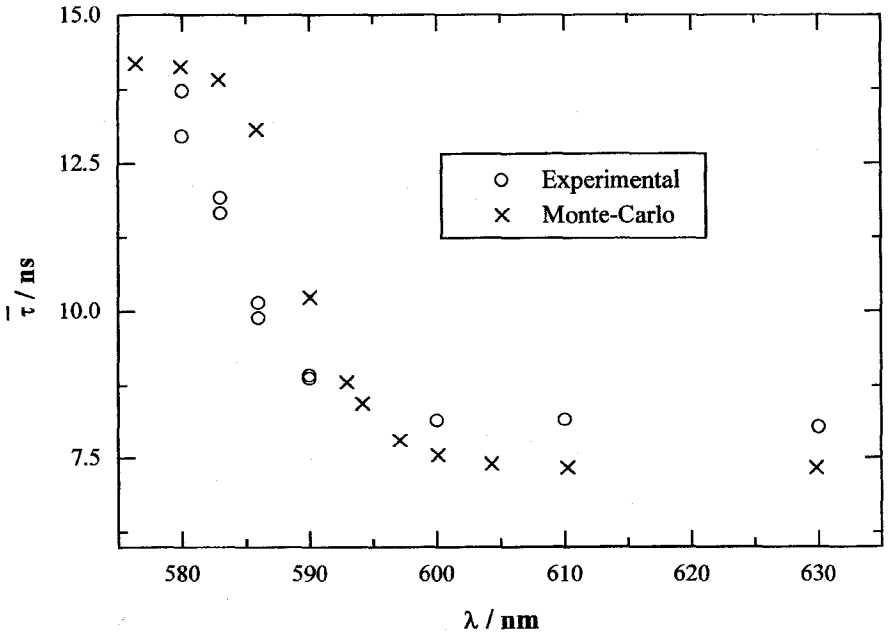

Figure 3.8 A comparison of experimental and predicted average lifetimes of 10^{-4} M solutions of rhodamine 101 for the right-angle geometry, as a function of the emission wavelength. Excitation wavelength 300 nm.

the fundamental mode of the Holstein–Biberman equation. This limiting distribution is centered in the middle of the cell and has approximately radial symmetry. Some tenth-generation distributions (see Plates 1 and 2) are already close to it.

3.5.2 Continuous excitation (photostationary state)

From Eqns 3.64 and 3.65 one may also obtain the steady state intensities,

$$\frac{I_b(\lambda)}{I_{0b}} = F(\lambda) \sum_{n=1}^{\infty} [1 - \alpha_{bn}(\lambda)] \left(\prod_{i=1}^{n-1} \bar{\alpha}_i \right) \Phi_0^{n-1}, \tag{3.67}$$

$$\frac{I_b}{I_{0b}} = \frac{\Phi_b}{\Phi_0} = \sum_{n=1}^{\infty} (1 - \bar{\alpha}_{bn}) \left(\prod_{i=1}^{n-1} \bar{\alpha}_i \right) \Phi_0^{n-1}, \tag{3.68}$$

$$\frac{I}{I_0} = \frac{\Phi}{\Phi_0} = \sum_{n=1}^{\infty}(1-\bar{\alpha}_n)\left(\prod_{i=1}^{n-1}\bar{\alpha}_i\right)\Phi_0^{n-1} = (1-\bar{\alpha}_1) + (1-\bar{\alpha}_2)\Phi_0\bar{\alpha}_1 + \ldots . \quad (3.69)$$

These equations may be compared with Eqns 3.34, 3.36, and 3.37. Note also that they can be converted into finite sums by means of approximations similar to that carried out for Eqn. 3.66.

3.5.3 Fluorescence anisotropy

It is well known that nonradiative transport decreases the ensemble fluorescence anisotropy. For a pair of randomly oriented and nonrotating molecules, and for the Förster dipolar mechanism, Galanin calculated in 1950 [1, 27] that the acceptor fluorescence anisotropy is only 4% of that of the donor. This result was later shown to be in fact the zero-time value of the indirectly excited molecule anisotropy [9]. In any event, neglect of the contribution of indirectly excited molecules to the ensemble anisotropy is a good and frequently made approximation in nonradiative transport studies, where theoretic efforts concentrate on calculation of the survival probability of directly excited molecules. This calculation is difficult on account of the possibility of excitation return. Nevertheless, good approximations ([6] and references therein), extensively tested experimentally (see, e.g., [5, 29]) are available.

The situation with radiative transport is, in a sense, the opposite of that with nonradiative transport. In fact, and owing to its long-ranged nature, the return of excitation has negligible probability. On the other hand, the contribution of indirectly excited molecules to the overall anisotropy is considerable, and cannot be neglected: the radiative mechanism has a higher orientational selectivity than the nonradiative one [3, 4]. For the purposes of computing the effect of radiative transport on fluorescence anisotropy, we consider only results for directions contained in the horizontal plane (including the usual front-face and right-angle geometries), for which the anisotropy of fluorescence takes the highest value. We further suppose that molecular rotational motion is negligible during the lifetime and that the exciting photons carry vertical polarization.

We start with the calculation of the depolarization due to radiative transfer of electronic excitation energy. To conform to usage, we write as r_0 the anisotropy of first- generation molecules (the fundamental anisotropy), implying that $r_1 = r_0$. The anisotropy of second-generation molecules, indirectly excited by reabsorption, will be

$$r_2 = \beta r_0, \quad (3.70)$$

where β is the depolarization factor ($\beta < 1$). In contrast to nonradiative transport, the probability of excitation return to the original molecule is negligible,

and therefore the anisotropy of fluorescence of molecules belonging to the nth generation is obtained by repeated application of Eqn 3.70:

$$r_n = \beta^{n-1} r_0 \qquad (n = 1, 2, \ldots). \tag{3.71}$$

A quantum-electrodynamical calculation of the depolarization factor β, by Andrews and Juzeliūnas [4], gave $\beta = 0.28$ (an identical value is obtained by classical electrodynamics [10]; see Appendix B). This value may be compared to that of the *nonradiative* dipole–dipole transfer mechanism, which is $\beta = 0.04$ [1, 4, 9, 27]. The polarization retained after one transfer is thus seven times greater for the radiative case – precluding, as mentioned above, the common approximation in nonradiative transport of neglecting the contribution of higher order generations.

For excitation with vertically polarized light, the definition of anisotropy is

$$r = \frac{I_{\parallel} - I_{\perp}}{I_{\parallel} + 2I_{\perp}}, \tag{3.72}$$

where the parallel and perpendicular intensities are measured for at right-angles to the excitation, and contained in the horizontal plane. The denominator of Eqn 3.72 is usually proportional to the intensity emitted in all directions. An alternative measure of linear polarization is the polarization p,

$$p = \frac{I_{\parallel} - I_{\perp}}{I_{\parallel} + I_{\perp}}, \tag{3.73}$$

where the denominator is the intensity emitted in the direction of measurement. In most fluorescence experiments, anisotropy is a more useful parameter than polarization, because the denominator is proportional to the intensity of decay, and simpler expressions result. When several incoherent sources are present (e.g. from a mixture of fluorescent compounds), both polarization and anisotropy can be expressed as a sum of contributions, the weight of each being the fraction of the intensity emitted in all directions (anisotropy), or the fraction of the intensity emitted in the direction of measurement (polarization).

When radiative transport is present, the denominator of Eqn 3.72 is no longer proportional to the intensity decay. In fact, the symmetry of the emitting ensemble is lowered, and a complicated positional pattern of polarizations emerges. Both anisotropy and polarization become local quantities (i.e. relative to the measurement point $\vec{r}_b$). From an experimental point of view, Eqn 3.72 can still be used. However, from a theoretic viewpoint, information is limited to the decay at a given boundary point (Eqn 3.64), which is proportional to $I_{\parallel}(t) + I_{\perp}(t)$ and not to $I_{\parallel}(t) + 2I_{\perp}(t)$ (both measured at $\vec{r}_b$). Polarization, as

given by Eqn 3.73, is therefore of more direct meaning. Nevertheless, given that anisotropy is the parameter used in the absence of radiative transport, it is important to obtain a generalized, albeit local anisotropy, that will reduce to the usual result in the limiting situation of negligible radiative transport. To do so, one takes into account the relation between the local anisotropy and local polarization,

$$p = \frac{3r}{2+r}, \tag{3.74}$$

or

$$r = \frac{2p}{3-p}. \tag{3.75}$$

The total polarization is first obtained:

$$p_b(\lambda, t) = \sum_{n=1}^{\infty} a_{bn}(\lambda, t) p_n, \tag{3.76}$$

where p_n is the polarization of the nth generation. From Eqns 3.71 and 3.74,

$$p_n = \frac{3\beta^{n-1} r_0}{2 + \beta^{n-1} r_0}. \tag{3.77}$$

The fractional contribution $a_{bn}(t)$ is

$$a_{bn}(\lambda, t) = \frac{I_{bn}(\lambda, t)}{I_b(\lambda, t)} = \left\{ [1 - \alpha_{bn}(\lambda)] \left(\prod_{i=1}^{n-1} \bar{\alpha}_i \right) \frac{(k_r t)^{n-1}}{(n-1)!} \right\} \Bigg/ \left\{ \sum_{n=1}^{\infty} [1 - \alpha_{bn}(\lambda)] \left(\prod_{i=1}^{n-1} \bar{\alpha}_i \right) \frac{(k_r t)^{n-1}}{(n-1)!} \right\}. \tag{3.78}$$

The polarization is therefore

$$p_b(\lambda, t) = \left\{ \sum_{n=1}^{\infty} [1 - \alpha_{bn}(\lambda)] \left(\prod_{i=1}^{n-1} \bar{\alpha}_i \right) \frac{(k_r t)^{n-1}}{(n-1)!} \frac{3\beta^{n-1} r_0}{2 + \beta^{n-1} r_0} \right\} \Bigg/ \left\{ \sum_{n=1}^{\infty} [1 - \alpha_{bn}(\lambda)] \left(\prod_{i=1}^{n-1} \bar{\alpha}_i \right) \frac{(k_r t)^{n-1}}{(n-1)!} \right\}, \tag{3.79}$$

and, finally, the anisotropy is obtained from Eqn 3.75:

$$r_b(\lambda, t) = r_0 \left\{ \sum_{n=1}^{\infty} [1 - \alpha_{bn}(\lambda)] \left(\prod_{i=1}^{n-1} \bar{\alpha}_i \right) \left(\frac{1}{2 + \beta^{n-1} r_0} \right) \frac{(k_r \beta t)^{n-1}}{(n-1)!} \right\} \Bigg/ \left\{ \sum_{n=1}^{\infty} [1 - \alpha_{bn}(\lambda)] \left(\prod_{i=1}^{n-1} \bar{\alpha}_i \right) \left(\frac{1}{2 + \beta^{n-1} r_0} \right) \frac{(k_r t)^{n-1}}{(n-1)!} \right\}. \tag{3.80}$$

By a reasoning similar to that for Eqn 3.66, it may be shown that for long times the anisotropy becomes

$$r_b(\lambda, t) \simeq r_0 \exp[-\bar{\alpha}_S (1 - \beta) k_r t]. \tag{3.81}$$

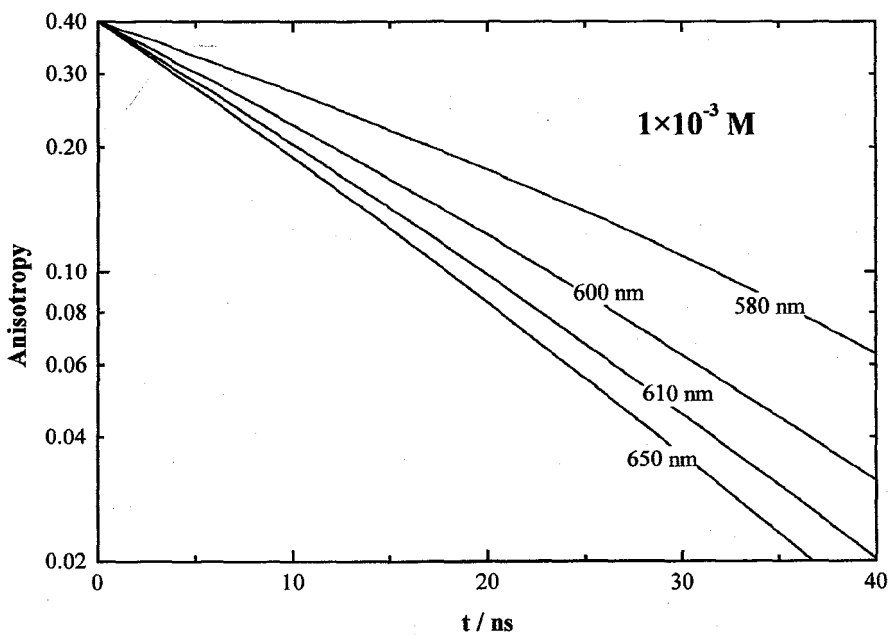

Figure 3.9 Theoretical anisotropy decays of 10^{-3} M rhodamine 101 in a rigid medium, front-face geometry, as a function of emission wavelength. Excitation wavelength 570 nm. (Reprinted with permission from E. J. Nunes Pereira, M. N. Berberan-Santos, and J. M. G. Martinho, *J. Chem. Phys.* 104 (1996) 8950. Copyright 1996 American Institute of Physics.)

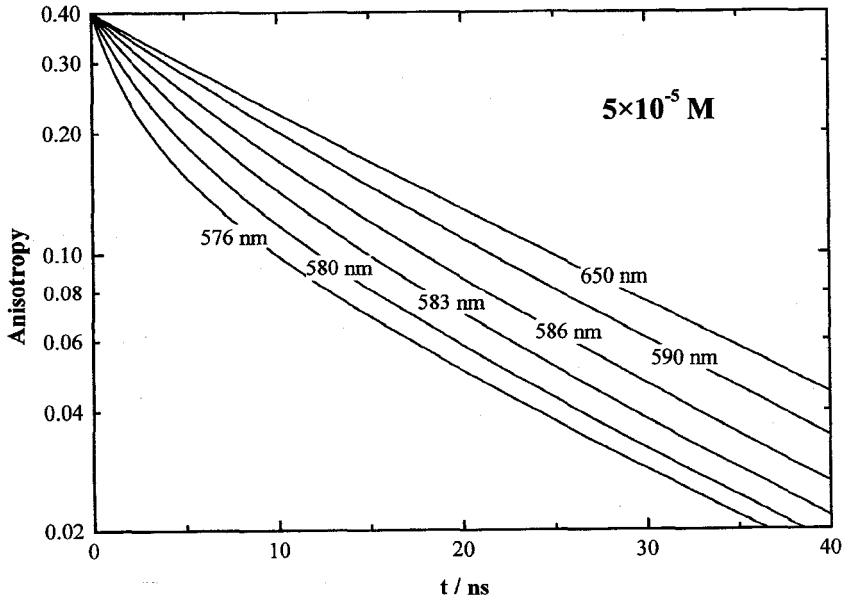

Figure 3.10 Theoretical anisotropy decays of 5×10^{-5} M rhodamine 101 in a rigid medium, right-angle geometry, as a function of emission wavelength. Excitation wavelength 300 nm. (Reprinted with permission from E. J. Nunes Pereira, M. N. Berberan-Santos and J. M. G. Martinho, *J. Chem. Phys.* 104 (1996), 8950, Copyright 1996 American Institute of Physics.)

Similarly, the polarization will then be

$$p_b(\lambda, t) \simeq \frac{3}{2} r_0 \exp[-\bar{\alpha}_S(1-\beta)k_r t]. \tag{3.82}$$

It should be stressed that the reabsorption probabilities of Eqns 3.79–3.82 must be computed with an absorption probability whose orientational dependence is that of a radiating electric dipole, and not that of an isotropic emitter, because it is now assumed that molecular rotation is frozen during the lifetime. However, the results are expected not to greatly differ.

Theoretical results for the anisotropy decay of rhodamine 101 in a rigid medium, computed from Eqn 3.80, are now presented. In Fig. 3.9 the decay is displayed for a 10^{-3} M solution and with front-face geometry. It is faster for "red" photons than for "blue" ones, because the latter are on average "younger", i.e. of a lower generation, than the "red" ones, and thus more polarized. In Fig. 3.10 the decay for a 5×10^{-5} M solution, with right-angle geometry, is displayed. Conversely, this is faster for "blue" photons than for "red" ones, because the latter are on average "older", i.e. of a higher generation, than the "red" ones, and thus less polarized.

3.6 COMBINED RADIATIVE AND NONRADIATIVE TRANSPORT

3.6.1 Importance of nonradiative transport

The contribution of nonradiative energy transport has been completely neglected up to now. Nonradiative transport will be present whenever the average distance between molecules is smaller or of the order of the Förster radius for self-transfer. Because some of the parameters that favor radiative transport (such as high absorption–emission spectral overlap and a high molecular radiative constant) also favor nonradiative transport by the dipole–dipole mechanism, the Förster radius for self-transfer tends to be significant. It is therefore important to discuss the effects of nonradiative transport on the macroscopic observables such as the fluorescence intensity decay, quantum yield and anisotropy decay.

In a system in which both mechanisms are operative and, neglecting coherence, the excitation will perform a series of short-range hops by the nonradiative mechanism, alternating with long-distance jumps by the radiative one. What conclusions can be drawn from this picture? First, it is well known that the decay law is unaffected by pure nonradiative transport [26]. In this way, each series of short hops will not change the decay probability of that sub-ensemble. Secondly, because the hops are performed locally, the excitation spread during the lifetime does not exceed a few Förster radii, and cannot change significantly the spatial distribution of the generations considered in the radiative model. An interesting consequence of the nonradiative hops is the efficient randomization of the orientation of the emitting dipole. In this way, and depending on the importance of the nonradiative mechanism, the assumption of isotropic emission may be appropriate even in cases in which molecular rotation is insignificant during the excited-state lifetime. All of these considerations lead to the conclusion that nonradiative transport leaves the decay law and quantum yield practically unchanged.

3.6.2 Fluorescence anisotropy

As regards the anisotropy decay, the contribution of nonradiative transport may be quite important. Invoking again the model of series of short hops alternating with long jumps, a strong depolarization is expected for each series of hops. Nonradiative transport will therefore contribute to the anisotropy decay – when significant, it may even be the dominant mechanism. It is thus of interest to obtain an expression for the combined effect of radiative and

nonradiative transport. To do so, we try to modify the anisotropy decay for pure radiative transport (Eqn 3.80). Following the nth radiative step, an $(n+1)$th-generation molecule is excited (at a certain time t_{n+1}). Owing to the nonradiative hops, there is a probability $G(t-t_{n+1})$ that the excitation will remain in that molecule. If the next radiative jump $(n+1 \rightarrow n+2)$ occurs from the initially excited molecule, one may still apply the depolarization equation (3.70). If, on the other hand, the radiative jump originates from an indirectly excited molecule by the nonradiative mechanism, total depolarization is expected. In this way, the emission probability for polarized emission will be, for each radiative step, $g(t)G(t)$, where $g(t)$ is given by Eqn A.2 and $G(t)$ is the probability that the excitation is in the directly excited molecule, when nonradiative transport is operative. The function $G(t)$ is given by several theoretic treatments. For three-dimensional rigid media, a simple but accurate formula is the so-called HHB approximation [6, 29]:

$$G(t) = \exp\left(-0.8452\, N_F \sqrt{\frac{\pi \Gamma t}{2}}\right), \tag{3.83}$$

where N_F is the average number of molecules contained in a sphere of radius equal to the Förster radius for self-transfer. In this way, the probability of the emission of polarized radiation by nth-generation molecules will be

$$g_n'(t) = \underbrace{gG \otimes gG \otimes \ldots \otimes gG}_{n\times}, \tag{3.84}$$

while the population of that generation will continue to be proportional to $g_n(t) = \Gamma[(\Gamma t)^{n-1}/(n-1)!]\mathrm{e}^{-\Gamma t}$ (see Appendix A). Hence, Eqn 3.71 is replaced by

$$r_n(t) = \beta^{n-1} r_0 \frac{g_n'(t)}{g_n(t)} \tag{3.85}$$

and Eqn 3.79 and 3.80 by

$$p_b(\lambda, t) = \left\{ \sum_{n=1}^{\infty} [1 - \alpha_{bn}(\lambda)] \left(\prod_{i=1}^{n-1} \bar{\alpha}_i \right) \left(\frac{3(\beta \Phi_0)^{n-1} r_0 g_n'(t)}{2 + \dfrac{g_n'(t)}{g_n(t)} \beta^{n-1} r_0} \right) \right\} \Bigg/ \left\{ \sum_{n=1}^{\infty} [1 - \alpha_{bn}(\lambda)] \left(\prod_{i=1}^{n-1} \bar{\alpha}_i \right) \Phi_0^{n-1} g_n(t) \right\}, \tag{3.86}$$

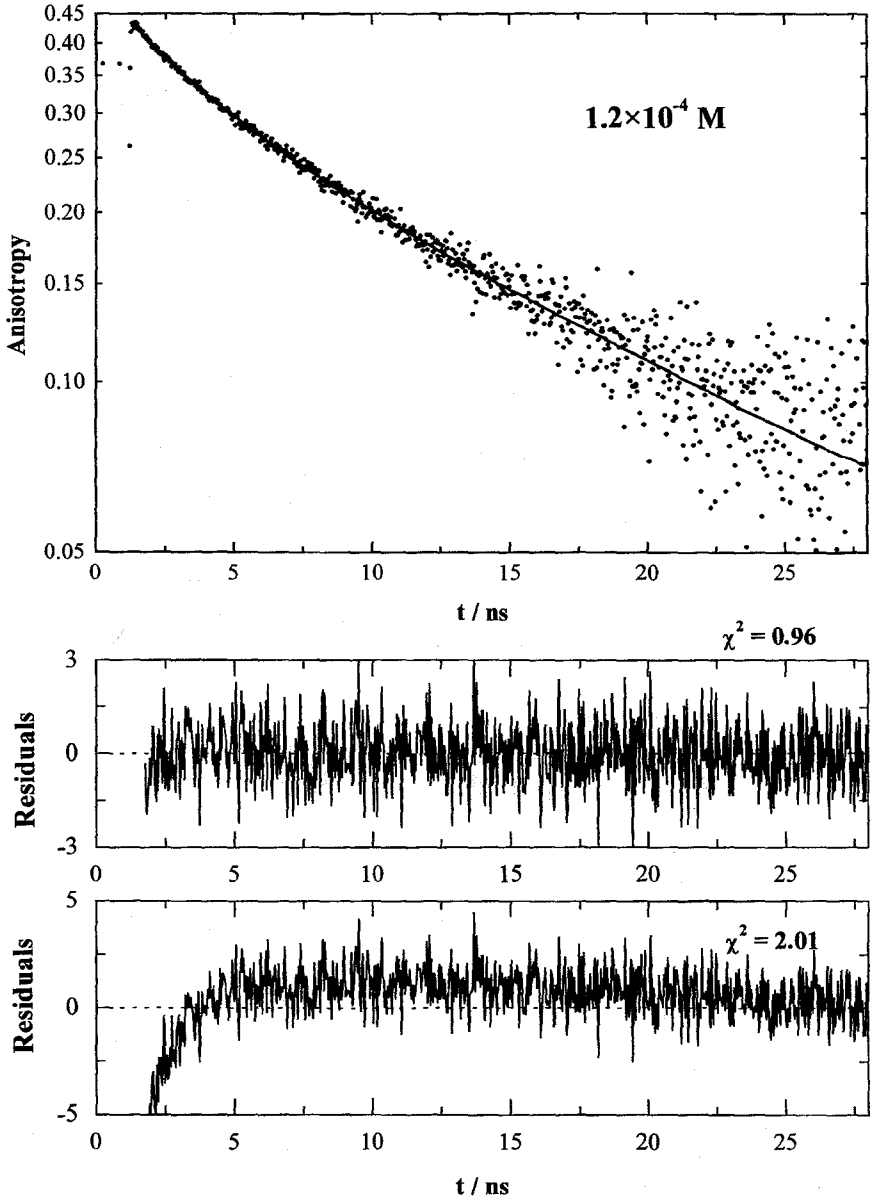

Figure 3.11 The fluorescence anisotropy decay of 1.2×10^{-4} M rhodamine 101 in acidified ethanol–methanol (9 : 1 v/v) at 100 K, right-angle geometry. The fit to Eqn 3.87, with due allowance for nonradiative transport, is quite good (upper residuals plot and reduced chi- squared value), while the fit to Eqn 3.80, where only radiative transport is considered, is clearly worse (lower residuals plot and reduced chi-squared value.)

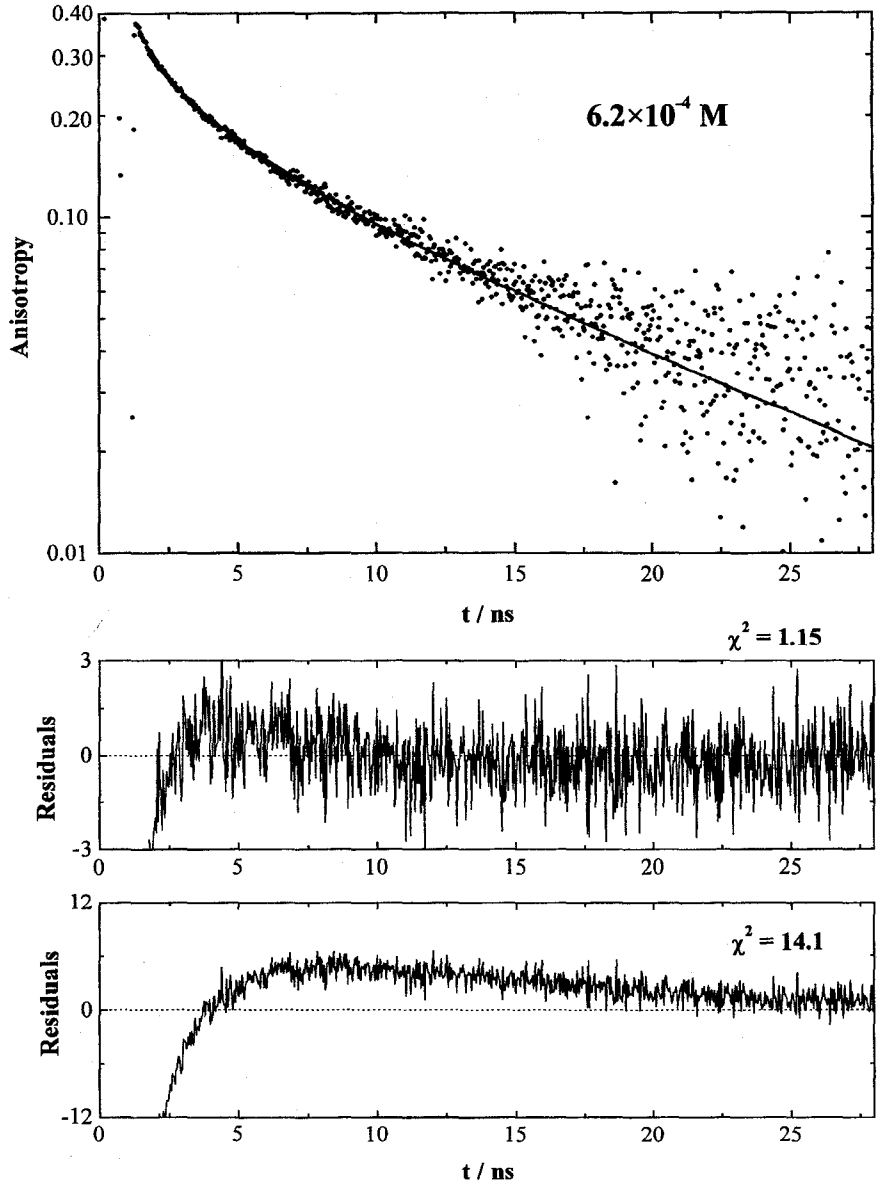

Figure 3.12 The fluorescence anisotropy decay of 6.2×10^{-4} M rhodamine 101 in acidified ethanol–methanol (9 : 1 v/v) at 100 K, right-angle geometry. The fit to Eqn 3.87, with due allowance for nonradiative transport, is good (upper residuals plot and reduced chi-squared value), while the fit to Eqn 3.80, where only radiative transport is considered, is much worse (lower residuals plot and reduced chi-squared value.)

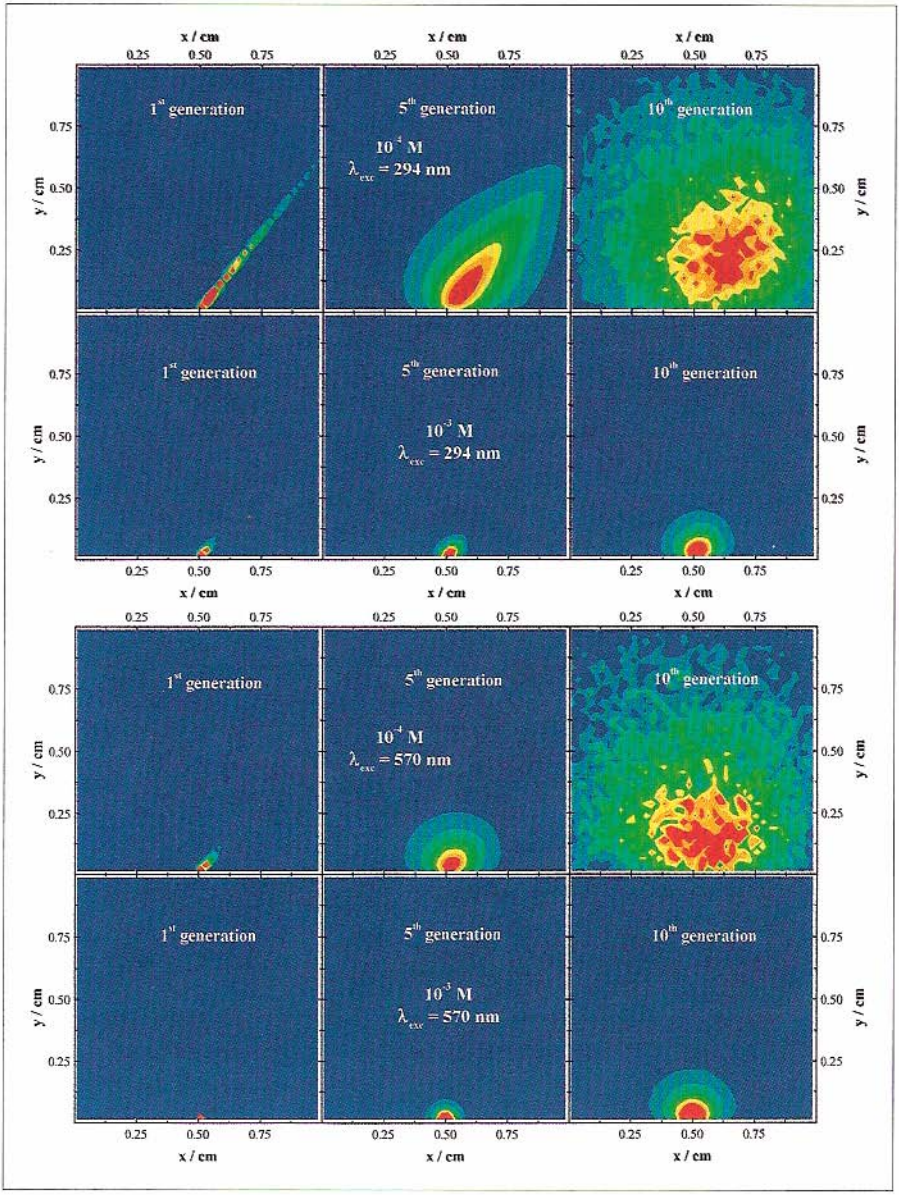

Plate 1 Spatial distribution functions for the first, fifth and tenth generations of excited molecules in a front-face geometry, obtained by Monte Carlo simulation. Reprinted with permission from E.J. Nunes Pereira, M.N. Berberan-Santos and J.M.G. Martinho, *J. Chem. Phys.* 104 (1996), 8950. Copyright 1996 American Institute of Physics.

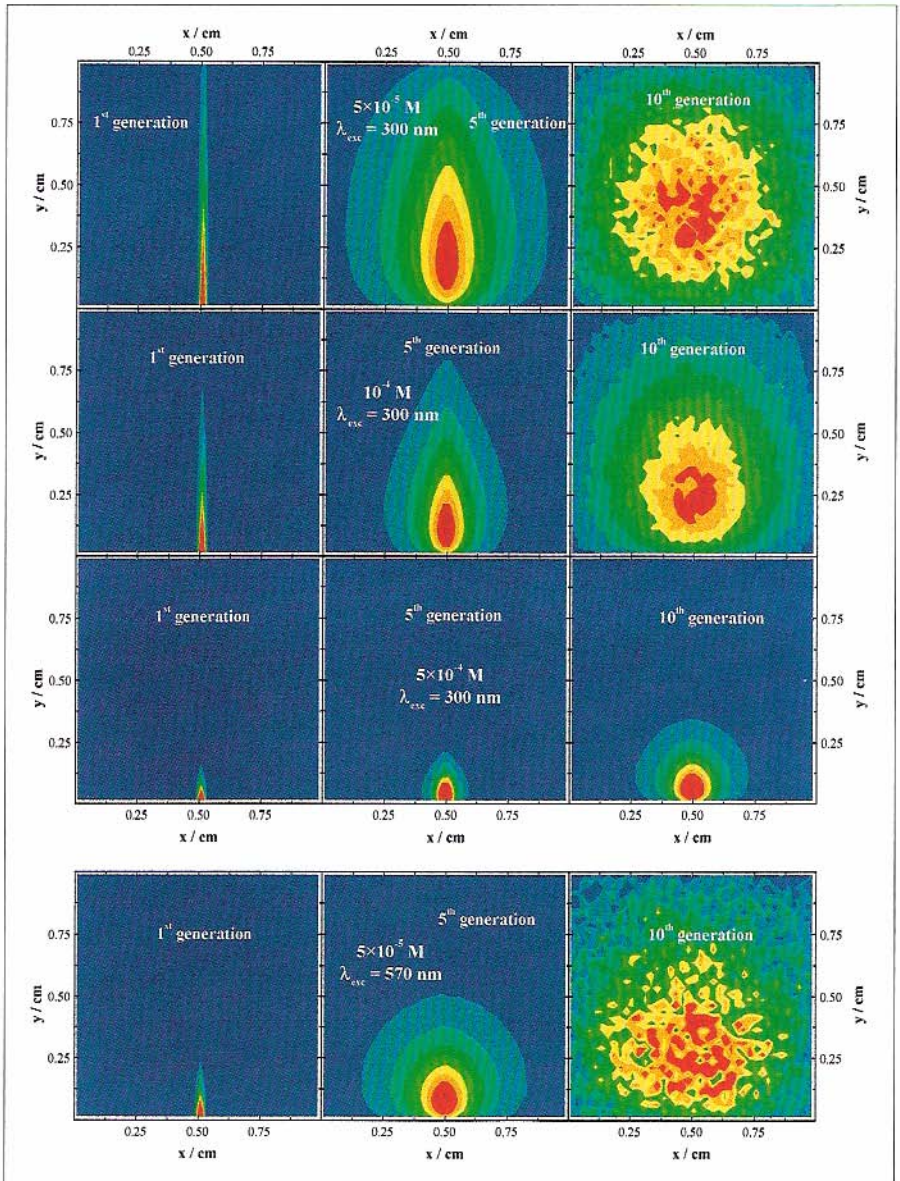

Plate 2 Spatial distribution functions for the first, fifth and tenth generations of excited molecules in a right-angle geometry, obtained by Monte Carlo simulation. Reprinted with permission from E.J. Nunes Pereira, M.N. Berberan-Santos and J.M.G. Martinho, *J. Chem. Phys.* 104 (1996), 8950. Copyright 1996 American Institute of Physics.

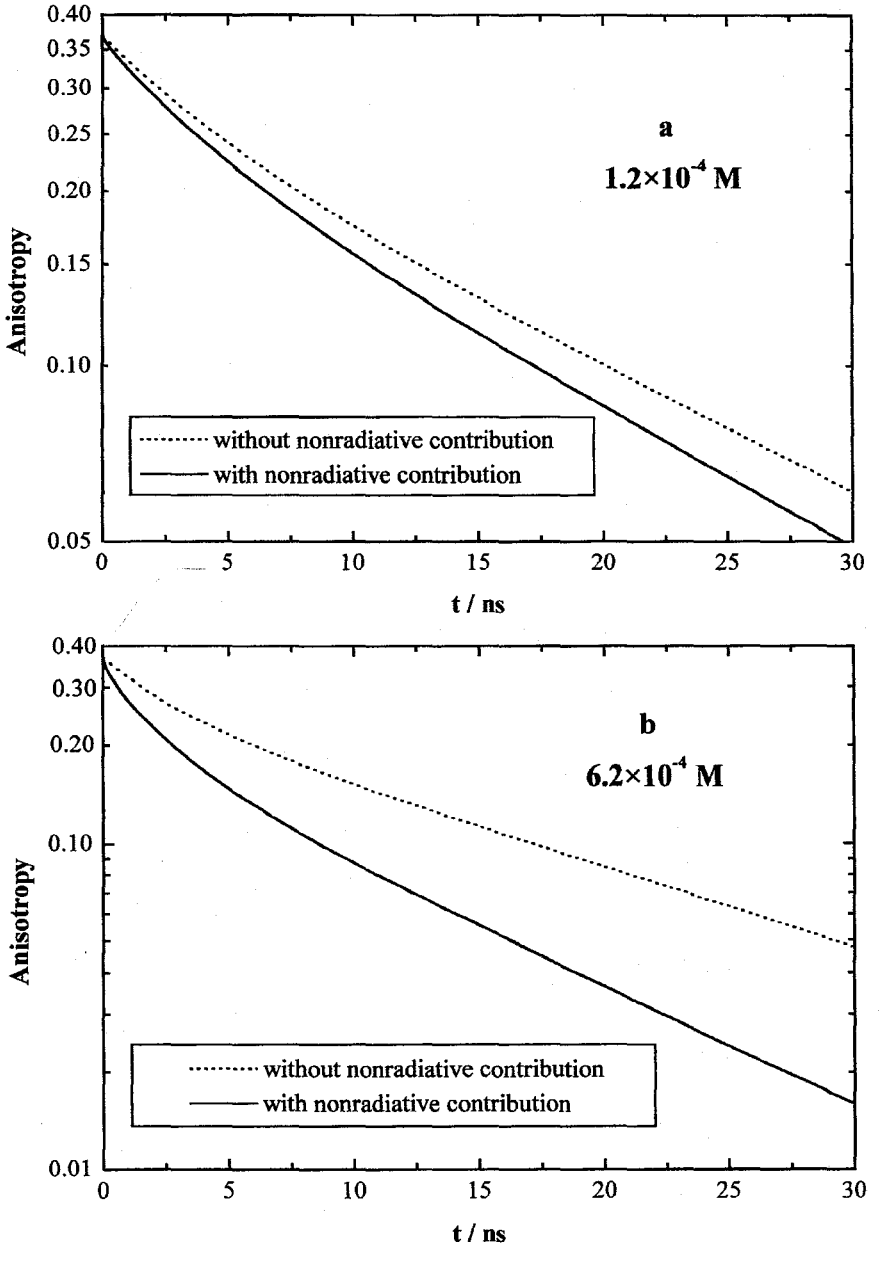

Figure 3.13 Theoretical anisotropy decays corresponding to Figs 3.11 and 3.12, but explicitly showing the effect of nonradiative transport.

$$r_b(\lambda, t) = r_0 \left\{ \sum_{n=1}^{\infty} [1 - \alpha_{bn}(\lambda)] \left(\prod_{i=1}^{n-1} \bar{\alpha}_i \right) \left(\frac{(\beta \Phi_0)^{n-1} g_n'(t)}{2 + \dfrac{g_n'(t)}{g_n(t)} \beta^{n-1} r_0} \right) \right\} \Bigg/ \left\{ \sum_{n=1}^{\infty} [1 - \alpha_{bn}(\lambda)] \left(\prod_{i=1}^{n-1} \bar{\alpha}_i \right) \left(\frac{\Phi_0^{n-1} g_n(t)}{2 + \dfrac{g_n'(t)}{g_n(t)} \beta^{n-1} r_0} \right) \right\}. \quad (3.87)$$

It must be remarked that the above considerations and formulas are not completely general. A unified treatment of the problem of combined radiative and nonradiative transport that includes the continuous variation from the r^{-6} interaction to the r^{-2} interaction [3] is wanting. We have considered only the combined effect of the (extreme) radiative and nonradiative (dipole–dipole) processes. Nevertheless, this is expected to be valid for most situations.

Some experimental time-resolved and steady state anisotropies for rhodamine 101 in an ethanol–methanol (9 : 1 v/v) glass at 100 K, for the right-angle geometry (cell edge detection), are now presented and briefly discussed. In Figs 3.11 and 3.12 the anisotropy decays of 1.2×10^{-4} M and 6.2×10^{-4} M solutions are displayed. In both cases, the fit to Eqn 3.87 (with due allowance for nonradiative transport) is good, while neglect of the nonradiative transport contribution leads to significantly worse fits, deviations being higher for the highest concentration. The effect of nonradiative transport is shown, in Fig. 3.13, to be especially important for the 6.2×10^{-4} M solution.

3.7 CONCLUSION

An integrated view of atomic and molecular radiative transport theories has been presented, stressing the similarities between the two fields. It has been shown that the two main treatments of radiative transport dynamics, one based on the Holstein–Biberman equation and the other on a stochastic formulation, are essentially equivalent. However, the latter appears to be physically clearer and more versatile – allowing, for instance, for consideration of the combined effect of radiative and nonradiative transport. The applicability of the theoretic results presented has, in several cases, been illustrated by comparison with experimental results.

Appendix A: Probability of emission of a photon between t and t + dt by an nth-generation molecule

In order to compute $g_n(t)$, it suffices to consider that the instant of emission for a given realisation of an n-step process is (neglecting at first the photon propagation time between molecules)

$$t = \sum_{i=1}^{n} \Delta t_i, \tag{A.1}$$

where Δt_i is the waiting time for the ith excited molecule involved in the sequence. Now the Δt_i are independent random variables with the common density function

$$g(\Delta t) = \Gamma \mathrm{e}^{-\Gamma \Delta t}. \tag{A.2}$$

Owing to the independence of the Δt_i, the random variable t has a density function given by the repeated convolution of Eqn A.2,

$$g_n(t) = \underbrace{g \otimes g \otimes \ldots \otimes g}_{n\times} = \Gamma \frac{(\Gamma t)^{n-1}}{(n-1)!} \mathrm{e}^{-\Gamma t}, \tag{A.3}$$

which is Eqn 3.56. The propagation time is neglected in this derivation. Its consideration is unnecessary for samples of a few centimeters, if the intrinsic decay lifetimes are of at least some nanoseconds. In such cases the decay times will be two or more orders of magnitude longer than the propagation times of individual hops ($1/c \sim 3$ ps/mm).

Appendix B: Depolarization factor for radiative transfer according to classical electrodynamics

Consider Fig. B.1. The depolarization factor β is given by [59, 63]

$$\beta = \frac{3\langle \cos^2 \omega \rangle - 1}{2}, \tag{B.1}$$

where ω is the angle formed by the transition moments of the donor and of the acceptor, and corresponds to the rotation of the transition dipole when the energy transfer occurs. This rotation can be thought to occur in two steps: first, the donor's transition moment rotates by an angle χ, becoming coincident with

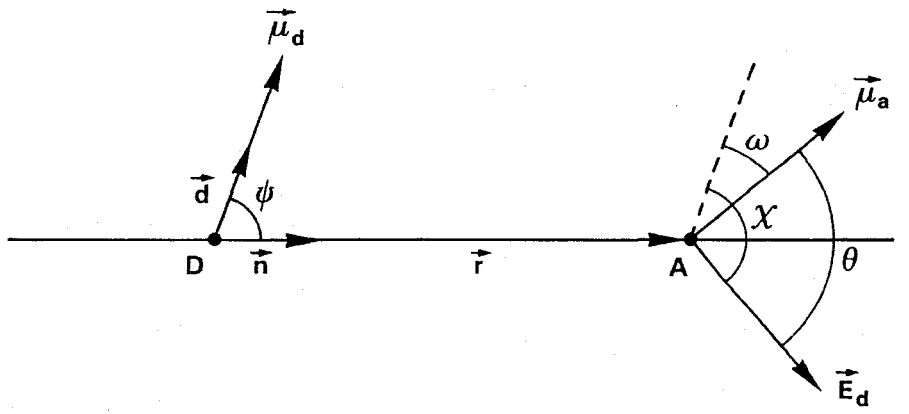

Figure B.1 A schematic representation of donor (D) and acceptor (A) relevant parameters for the computation of the depolarization factor: $\vec{\mu}_d$ and $\vec{\mu}_a$ are the donor and acceptor transition moments, $\vec{d}$ and $\vec{n}$ are the unit vectors along the transition moment of the donor and along the direction joining D and A, and $\vec{E}_d$ is the electric field of the donor at the acceptor. (Reprinted with permission from M. N. Berberan-Santos, E. J. Nunes Pereira, and J. M. G. Martinho, *J. Chem. Phys.* 103 (1995) 3022. Copyright 1995 American Institute of Physics.)

the direction of the electric field of the donor at the acceptor; it then rotates again by an angle θ so as to coincide with the direction of the acceptor's transition moment. Because these two angles are independent (χ depends only on the orientation of the donor; θ depends only on the orientation of the acceptor; and the donor and acceptor have uncorrelated orientations) Eqn B.1 can be rewritten as a product of two Soleillet factors [59, 63]:

$$\beta = \frac{3\langle\cos^2\omega\rangle - 1}{2} = \frac{3\langle\cos^2\chi\rangle - 1}{2} \times \frac{3\langle\cos^2\theta\rangle - 1}{2}. \tag{B.2}$$

The electric field of the donor at the acceptor is, for the radiative zone,

$$\vec{E}_d = C\left[(\vec{n}\cdot\vec{d})\vec{n} - \vec{d}\right] = C(\cos\psi\,\vec{n} - \vec{d}), \tag{B.3}$$

C being a distance-dependent factor. Now the absorption probability is proportional to

$$|\vec{E}_d \cdot \vec{\mu}_a|^2 \propto |\vec{E}_d|^2\cos^2\theta = \sin^2\psi\cos^2\theta. \tag{B.4}$$

Because the orientational distribution function for the donor is

$$f(\psi) = \sin \psi, \qquad \psi \in \left[0, \frac{\pi}{2}\right] \tag{B.5}$$

and given Eqn B.4, the ψ orientational distribution for pairs with excited acceptors will be

$$g(\psi) = \frac{3}{2}\sin^3 \psi. \tag{B.6}$$

On the other hand,

$$\cos \chi = \frac{\vec{d} \cdot \vec{E}_d}{|\vec{E}_d|} = -\sin \psi; \tag{B.7}$$

hence

$$\langle \cos^2 \chi \rangle = \langle \sin^2 \psi \rangle = \int_0^{\frac{\pi}{2}} \sin^2 \psi \, g(\psi) \mathrm{d}\psi = \frac{4}{5}. \tag{B.8}$$

In the same way, the θ distribution function for pairs with excited acceptors will be

$$g(\theta) = \frac{3}{2}\cos^2 \theta \sin \theta \tag{B.9}$$

and therefore

$$\langle \cos^2 \theta \rangle = \int_0^{\pi} \cos^2 \theta \, g(\theta) \mathrm{d}\theta = \frac{3}{5}. \tag{B.10}$$

Finally, from Eqns B.2, B.8, and B.10, the depolarization factor is

$$\beta = \frac{7}{10} \times \frac{2}{5} = \frac{7}{25} = 0.28. \tag{B.11}$$

References

1. Agranovich, V. M., and M. D. Galanin 1982. *Electronic Excitation Energy Transfer in Condensed Matter*. North-Holland, Amsterdam.
2. Alpert, D., A.O. McCoubrey, and T. Holstein 1949. Imprisonment of resonance radiation in mercury vapor. *Phys. Rev.* 76: 1257–1259.
3. Andrews, D. L., and P. Allcock 1995. Bimolecular photophysics. *Chem. Soc. Rev.* 24: 259–265.
4. Andrews, D. L., and G. Juzeliūnas 1991. The range dependence of fluorescence anisotropy in molecular energy transfer. *J. Chem. Phys.* 95: 5513–5518.
5. Anfinrud, P. A., D. E. Hart, J. F. Hedstrom, and W. S. Struve 1986. Fluorescence depolarization of rhodamine 6G in glycerol: a photon-counting test of three-dimensional excitation transport theory. *J. Phys. Chem.* 90: 2374–2379.
6. Baumann, J., and M.D. Fayer 1985. Excitation transfer in disordered two-dimensional and anisotropic three-dimensional systems: effects of spatial geometry on time-resolved observables. *J. Chem. Phys.* 85: 4087–4107.
7. Baumann, J., G. Calzaferri, and T. Hugentobler 1985. Self-absorption and re-emission in wavelength-dependent fluorescence decay. *Chem. Phys. Lett.* 116: 66–72.
8. Berberan-Santos, M. N., and J. M. G. Martinho 1992. A linear response approach to kinetics with time-dependent rate coefficients. *Chem. Phys.* 164: 259–269.
9. Berberan-Santos, M. N., and B. Valeur 1991. Fluorescence depolarization by electronic energy transfer in donor–acceptor pairs of like and unlike chromophores. *J. Chem. Phys.* 95: 8048–8055.
10. Berberan-Santos, M. N., E. J. Nunes Pereira, and J. M. G. Martinho 1995. Stochastic theory of molecular radiative energy transport. *J. Chem. Phys.* 103: 3022–3028.
11. Berberan-Santos, M. N., E. J. Nunes Pereira, and J. M. G. Martinho 1997. Stochastic theory of combined radiative and non-radiative energy transport. *J. Chem. Phys.* 107: 10 480–10 484.
12. Biberman, L. M. 1947. On the theory of the diffusion of resonance radiation. *Zh. Eksperim. i Teor. Fiz.* 17: 416–426 [*Sov. Phys. JETP* 19, 584, 1949].
13. Birks, J. B. 1953. *Scintillation Counters*. Pergamon Press, London.
14. Birks, J. B. 1954. Energy transfer in organic phosphors. *Phys. Rev.* 94: 1567–1573.
15. Birks, J. B. 1964. *The Theory and Practice of Scintillation Counting*. Pergamon Press, Oxford.
16. Birks, J. B. 1970. *Photophysics of Aromatic Molecules*. John Wiley, London.
17. Birks, J. B. 1974. The influence of reabsorption and defects on anthracene crystal fluorescence. *Mol. Cryst. Liq. Cryst.* 28: 117–129.
18. Birks, J. B. 1975. Photophysics of aromatic molecules – a postscript. In *Organic Molecular Photophysics*. J. B. Birks, editor. John Wiley, London, Vol. 2.
19. Birks, J. B., and I. H. Munro 1967. The fluorescence lifetimes of aromatic molecules. *Prog. React. Kinet.* 4: 239–303.
20. Blickensderfer, R. P., W. H. Breckenridge, and J. Simons 1976. Diffusion theory of imprisonment of atomic resonance radiation at low opacities. *J. Phys. Chem.* 80: 653–659.
21. Braun, M., H. Liening, B. Storr, and P. Wiorkowski 1985. Comparison of experiments and theory in time resolved fluorescence spectroscopy. *Opt. Commun.* 53: 221–224.
22. Calvert, J. G., and J. N. Pitts Jr. 1966. *Photochemistry*. John Wiley, New York.
23. Compton, K. T. 1923. Some properties of resonance radiation and excited atoms. *Phil. Mag.* 45: 750–760.

24. Dhami, S., A. J. de Mello, G. Rumbles, S. M. Bishop, D. Phillips, and A. Beeby 1995. Phthalocyanine fluorescence at high concentration: dimers or reabsorption effect? *Photochem. Photobiol.* 61: 341–346.
25. Falecki, W., W. Hartmann, and R. Bocksch 1991. New aspects of Holstein's treatment of radiation trapping. *Opt. Commun.* 83: 215–219.
26. Förster, Th. 1948. Zwischenmolekulare Energiewanderung und Fluoreszenz. *Ann. Phys. (Leipzig)* 2: 55–75.
27. Galanin, M. D. 1996. *Luminescence of Molecules and Crystals.* Cambridge International Science Publishing, Cambridge.
28. Hammond, P. R. 1979. Self-absorption of molecular fluorescence, the design of equipment for measurement of fluorescence decay, and the decay times of some laser dyes. *J. Chem. Phys.* 70: 3884–3894.
29. Hart, D. E., P. A. Anfinrud, and W. S. Struve 1987. Excitation transport in solution: a quantitative comparison between GAF theory and time-resolved fluorescence profiles. *J. Chem. Phys.* 86: 2689–2696.
30. Holstein, T. 1947. Imprisonment of resonance radiation in gases. *Phys. Rev.* 72: 1212–1233.
31. Holstein, T. 1951. Imprisonment of resonance radiation in gases. II. *Phys. Rev.* 83: 1159–1168.
32. Huennekens, J., and A. Gallagher 1983. Radiation diffusion and saturation in optically thick Na vapor. *Phys. Rev. A.* 28: 238–247.
33. Kawahigashi, M., and S. Hirayama 1989. Microscopic fluorescence decay measurements on thin liquid films and droplets of concentrated dye solutions. *J. Luminescence* 43: 207–212.
34. Kenty, C. 1932. On radiation diffusion and the rapidity of escape of resonance radiation from a gas. *Phys. Rev.* 42: 823–842.
35. Kilin, S. F., and I. M. Rozman 1959. Effect of reabsorption on the fluorescence lifetimes of organic substances. *Opt. Spectrosc.* 6: 40–44.
36. Lai, R., S. Liu, and X. Ma 1993. Theoretical treatment of resonance radiation imprisonment: new approach to Holstein's equation. *Z. Phys. D* 27: 223–228.
37. Lipsett, F. R. 1967. The quantum efficiency of luminescence. *Progr. Dielectrics* 7: 217–319.
38. Ma, X., and R. Lai 1994. Theoretical treatment of radiation trapping: steady-state conditions and quenching experiment. *Phys. Rev. A* 49: 787–793.
39. Malyshev, V. A., and V. L. Shekhtman 1978. Trapping of radiation in an activated condensed medium. *Sov. Phys. – Solid State* 20: 1684–1691.
40. Martinho, J. M. G., and J. M. R. d'Oliveira 1990. Influence of radiative transport on energy transfer. *J. Chem. Phys.* 93: 3127–3132.
41. Martinho, J. M. G., A. L. Maçanita, and M. N. Berberan-Santos 1989. The effect of radiative transport on fluorescence emission. *J. Chem. Phys.* 90: 53–59.
42. Melhuish, W. H. 1961. Quantum efficiencies of fluorescence of organic substances: effect of solvent and concentration of the fluorescent solute. *J. Phys. Chem.* 65: 229–235.
43. Milne, E. A. 1926. The diffusion of imprisoned radiation through a gas. *J. London Math. Soc.* 1: 40–51.
44. Molisch, A. F., B. P. Ohery, and G. Magerl 1992. Radiation-trapping in a plane-parallel slab. *J. Quant. Spectrosc. Radiat. Transfer* 48: 377–396.
45. Molisch, A. F., B. P. Ohery, W. Schupita, and G. Magerl 1993. Radiation-trapping in cylindrical and spherical geometries. *J. Quant. Spectrosc. Radiat. Transfer* 49: 361–370.

67. Wood, R. W. 1912. Selective reflexion, scattering and absorption by resonating gas molecules. *Phil. Mag. J. Sci.* 23: 689–714.
68. Zemansky, M. W. 1927. The diffusion of imprisoned resonance radiation in mercury vapor. *Phys. Rev.* 29: 513–523.